

Interim Report Hanford Tanks AY-102 and AP-101: Effect of Chemistry and Other Variables on Corrosion and Stress Corrosion Cracking

M.H. Harty
CH2M HILL Hanford Group, Inc.
Richland, WA 99352
U.S. Department of Energy Contract DE-AC27-99RL14047

EDT/ECN: N/A UC: N/A
Org Code: N/A Charge Code:
B&R Code: N/A Total Pages: *40*

Key Words: Corrosion, Stress Corrosion Cracking, Tank AY-102, Tank AP-101, Chemistry

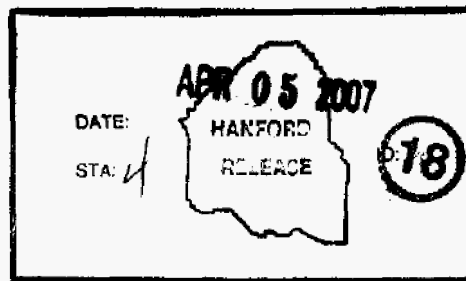
Abstract: The objective of this work is to determine the range of conditions where the tank steel is susceptible to localized corrosion and SCC in simulants for waste in tanks AY-102 and AP-101.

TRADEMARK DISCLAIMER. Reference herein to any specific commercial product, process, or service by trade name, trademark, manufacturer, or otherwise, does not necessarily constitute or imply its endorsement, recommendation, or favoring by the United States Government or any agency thereof or its contractors or subcontractors.

Printed in the United States of America. To obtain copies of this document, contact: Document Control Services, P.O. Box 950, Mailstop H6-08, Richland WA 99352, Phone (509) 372-2420; Fax (509) 376-4989.

M.E. Bratton *4/5/07*

Release Approval Date



Release Stamp

Approved for Public Release

RPP-RPT-31932 Rev.0

RPP-RPT-31932
Rev. 0

**INTERIM REPORT 8117013
HANFORD TANKS AY-102 AND AP-101: EFFECT OF CHEMISTRY AND
OTHER VARIABLES ON CORROSION AND STRESS CORROSION
CRACKING**

Author Names: C. Sean Brossia PhD, Colin Scott PhD, Feng Gui PhD
CC Technologies, Dublin, Ohio for ARES Corporation for
CH2M HILL Hanford Group, Inc.

Date Published
March 30, 2007



Prepared for the U.S. Department of Energy
Office of River Protection

Contract #DE-AC27-99RL14047, Modification M030

Approved for Public Release; Further Dissemination Unlimited

RPP-RPT-31932, Rev. 0

INTERIM REPORT
8117013

**HANFORD TANKS AY-102 AND AP-101:
EFFECT OF CHEMISTRY AND OTHER VARIABLES ON CORROSION
AND STRESS CORROSION CRACKING**

PREPARED FOR
ARES CORPORATION
RICHLAND, WASHINGTON

PREPARED BY
CC TECHNOLOGIES, INC.
CORROSION AND MATERIALS TECHNOLOGY LABORATORY
C. SEAN BROSSIA, PH.D.
COLIN SCOTT, PH.D., P.ENG.
FENG GUI, PH.D.

MARCH 30, 2007



CC Technologies
A DNV COMPANY
Innovative Solutions

5777 FRANTZ ROAD
DUBLIN, OHIO 43017
614.761.1214 • 614.761.1633 fax
www.cctechnologies.com

RPP-RPT-31932, Rev. 0

Hanford Tanks AY-102 and AP-101: Corrosion and Stress Corrosion Cracking

Interim Report

SIGNATURE PAGE

FIRST AUTHOR:

C. Sean Brossia
Director of Research

CSBrossia

Date March 30, 2007

REVIEWED BY:

Oliver C. Moghissi
Sr. Vice President - Laboratories

Oliver C. Moghissi

Date March 30, 2007

APPROVED BY:

Oliver C. Moghissi
Sr. Vice President - Laboratories

Oliver C. Moghissi

Date March 30, 2007

RPP-RPT-31932, Rev. 0

Hanford Tanks AY-102 and AP-101: Corrosion and Stress Corrosion Cracking

Interim Report

DISCLAIMER

This report documents work performed by CC Technologies, Inc. (CC Technologies) Dublin, Ohio, for ARES Corporation, Richland, Washington. Neither CC Technologies nor any person acting on behalf of CC Technologies:

- assumes any liability for consequences or damages resulting from the use, misuse, or reliance upon the information disclosed in this report.
- makes any warranty or representations that the use of any information, apparatus, method, or process disclosed in this report may not infringe on privately-owned rights.

EXECUTIVE SUMMARY

The Hanford tank reservation contains approximately 50 million gallons of liquid legacy radioactive waste from cold war weapons production, which is stored in 177 underground storage tanks. Current plans call for eventual vitrification processing and ultimate disposal of the resulting waste glass logs at the Yucca Mountain Repository. The double shelled carbon steel tanks presently used for storage will continue in operation until the vitrification plant construction is finalized and waste processing operations completed. Due to various chemical reactions taking place inside the tank, the waste chemistry will tend to change over time, especially given the currently estimated 2023 time horizon anticipated for tank operations to continue. In addition, the present chemistries for some of the tank waste types are no longer in specification with respect to corrosion mitigation (e.g., maintaining pH levels above 13). Thus, there is concern within DOE and regulatory bodies that tank integrity will be compromised given these changes in chemistry. Furthermore, if tank integrity is potentially compromised, there is a need to define mitigation procedures. Thus, the objective of this work is to determine the range of conditions where the tank steel is susceptible to localized corrosion and SCC in simulants for wastes in tanks AY-102 and AP-101.

Based on the work conducted during Phase 1 of the program, the key findings of the research are:

- No pitting corrosion was observed in either AY-102 at pH 11 or AP-101 at pH 14+ even at very high potentials, and this appears independent of the testing temperature
- The CPP curves at 50°C and at 77°C in both simulants showed no appreciable differences resulting from the increase in temperature
- The OCP in AY-102 was much more negative than that observed in AN107 likely because water reduction was the dominant cathodic reaction in AY-102
- The presence of oxygen shifted the OCP in the noble (higher potential) direction in AY-102 primarily because the oxygen reduction reaction was the dominant cathodic reaction
- Increasing the temperature from 50°C to 77°C did not appreciably change the susceptibility to SCC in AY-102, but slightly increased cracking susceptibility in AP-101 at 77°C
- SCC seemed to be relatively minor in both AY-102 and AP-101 and no severe cracking has been observed in the pH range and the applied potential range being evaluated
- Cracking appeared to be slightly worse at 0 mV and at potentials below the active-passive transition potential observed on CPP curves in AY-102 at 77°C (i.e. the "nose" potential); at 50°C, cracking was only observed at potentials more negative than -750 mV

RPP-RPT-31932, Rev. 0

Hanford Tanks AY-102 and AP-101: Corrosion and Stress Corrosion Cracking

Interim Report

CONTENTS

INTRODUCTION AND BACKGROUND.....	7
SUMMARY OF KEY FINDINGS.....	9
EXPERIMENTAL APPROACH	10
Materials and Specimens.....	10
Chemicals and Solutions	11
Open Circuit Potential Monitoring and Cyclic Potentiodynamic	13
Polarization Testing	13
Slow Strain Rate Testing	13
RESULTS AND DISCUSSION.....	15
Electrochemical Polarization Behavior.....	15
Summary of Electrochemical Behavior.....	21
Slow Strain Rate Testing	21
Summary of SSRT Testing	25
APPENDIX A.....	26
Photographs of Cyclic Potentiodynamic Polarization Test Specimens	26
APPENDIX B.....	28
Photographs of Slow Strain Rate Test Specimens	28

INTRODUCTION AND BACKGROUND

The Hanford tank reservation contains approximately 50 million gallons of liquid legacy radioactive waste from cold war weapons production, which is stored in 177 underground storage tanks. Current plans call for eventual vitrification processing and ultimate disposal of the resulting waste glass logs at the Yucca Mountain Repository. The double shelled carbon steel tanks presently used for storage will continue in operation until the vitrification plant construction is finalized and waste processing operations completed.

Though there are several different waste chemistry types that have been grouped according to their main constituents, all of the wastes tend to be highly alkaline in nature, typically with pH values greater than 10 and as high as 14. Under alkaline conditions, carbon steels will tend to be passive and undergo relatively slow, uniform corrosion. Under these passive conditions, however, carbon steels also can become susceptible to localized corrosion (e.g., pitting) and stress corrosion cracking (SCC) in the presence of certain aggressive constituents, such as chloride and nitrate. The original single shell storage tanks experienced stress corrosion cracking failures as a result of the presence of high concentrations of nitrate in the waste. Research at Hanford and SRL demonstrated that cracking could be prevented by maintaining a high pH of the waste (>13) and stress relieving the welds in the tanks. Accordingly, all of the double shelled storage tanks were fabricated with stress relieved welds and chemistry controls were instituted to maintain the pH of the waste above 13.5.

Due to various chemical reactions taking place inside the tank, the waste chemistry will tend to change over time, especially given the currently estimated 2023 time horizon anticipated for tank operations to continue. In addition, the present chemistries for some of the tank waste types are no longer in specification with respect to corrosion mitigation (e.g., maintaining pH levels above 13). Thus, there is concern within DOE and regulatory bodies that tank integrity will be compromised given these changes in chemistry. Furthermore, if tank integrity is potentially compromised, there is a need to define mitigation procedures.

Research conducted at CCT for Tank AN-107¹ revealed that pH did not have significant impact on either localized corrosion or SCC of carbon steel in the range of 10 to 13.5. It was found that a nitrite concentration above 1.2 M considerably reduced the susceptibility of carbon steel to pitting corrosion and SCC. Furthermore, the nitrite concentration is gradually increasing in the AN-107 waste from the present concentration of 1.2M to 2.4M in the predicted endpoint chemistry. Thus, the tank chemistry in AN-107 seems to be self-inhibiting because of the good inhibition from nitrite. As a result, it appeared to be unnecessary to adjust the pH back to the high levels required by the specifications (i.e. over 13).

¹ "Hanford tanks 241-AN-107 and 241-AN-102: Effect of Chemistry and Other Variables on Corrosion and Stress Corrosion Cracking", CC Technologies Inc, September 8, 2006.

RPP-RPT-31932, Rev. 0

Hanford Tanks AY-102 and AP-101: Corrosion and Stress Corrosion CrackingInterim Report

With reference to Tanks AY-102 and AP-101, the present pH is at 11 and over 13, respectively. The chemistry in these tanks is different from that in AN-107. The AY-102 is a carbonate based chemistry and only has very concentrations of nitrate and nitrite. The AP-101 is a nitrate based chemistry with some species that were not present in AN-107. Because of these differences, there is some uncertainty as to the direct applicability of the previous results obtained for AN-107. It is expected, however, that some general observations and interrelationships should be achievable.

The present work consists of two phases. The objective of Phase 1 was to obtain some initial understanding on the behavior of carbon steel in AY-102 and AP-101 simulants. Phase 2 then involves extensive testing of the critical factors to provide a more comprehensive understanding of the behavior of carbon steel with respect to localized corrosion and SCC. Based on the results, it is expected decisions can be made regarding the need of corrosion mitigation strategies for AY-102 and AP-101. This interim report describes the experimentation and results from Phase 1. A final report will be issued to describe the results of the entire project including Phase 2 once all testing is completed.

SUMMARY OF KEY FINDINGS

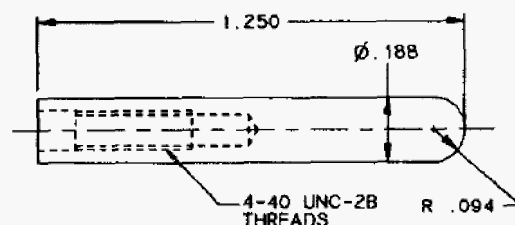
Based on the work conducted during Phase 1 of the program, the key findings of the research are:

- No pitting corrosion was observed in either AY-102 at pH 11 or AP-101 at pH 14+ even at very high potentials, and this appears independent of the testing temperature
- The CPP curves at 50°C and at 77°C in both simulants showed no appreciable differences resulting from the increase in temperature
- The OCP in AY-102 was much more negative than that observed in AN107 likely because water reduction was the dominant cathodic reaction in AY-102
- The presence of oxygen shifted the OCP in the noble (higher potential) direction in AY-102 primarily because the oxygen reduction reaction was the dominant cathodic reaction
- Increasing the temperature from 50°C to 77°C did not appreciably change the susceptibility to SCC in AY-102, but slightly increased cracking susceptibility in AP-101 at 77°C
- SCC seemed to be relatively minor in both AY-102 and AP-101 and no severe cracking has been observed in the pH range and the applied potential range being evaluated
- Cracking appeared to be slightly worse at 0 mV and at potentials below the active-passive transition potential observed on CPP curves in AY-102 at 77°C (i.e. the "nose" potential); at 50°C, cracking was only observed at potentials more negative than -750 mV

EXPERIMENTAL APPROACH

Materials and Specimens

All test specimens were fabricated from one 2'x2'x1" as-supplied plate of AAR TC 128 Grade B tank car steel which is believed to be similar to the steel used in tank construction. Three main specimen geometries are utilized in this work, as shown in FIGURES 1 – 3. Specimens were fabricated by Metal Samples Company in Munford, AL and Metcut Research, Inc. in Cincinnati, OH. Material close to the flame cuts at the edges of the plates was avoided for specimen fabrication to ensure consistent microstructures. The slow strain rate test (SSRT) specimens were fabricated such that the longitudinal axis was in the plate rolling direction (i.e., longitudinal orientation). Compact tension (CT) specimens were fabricated such that the pre-crack was in the plate rolling direction (i.e., transverse-longitudinal orientation). The CT specimens were not used in this phase of the work, but were machined in preparation for the continuing Phase 2 work.



SURFACE FINISH - APPROXIMATELY 8-16 RMS.

Figure 1. Engineering drawing of the CPP specimen (units in inches)

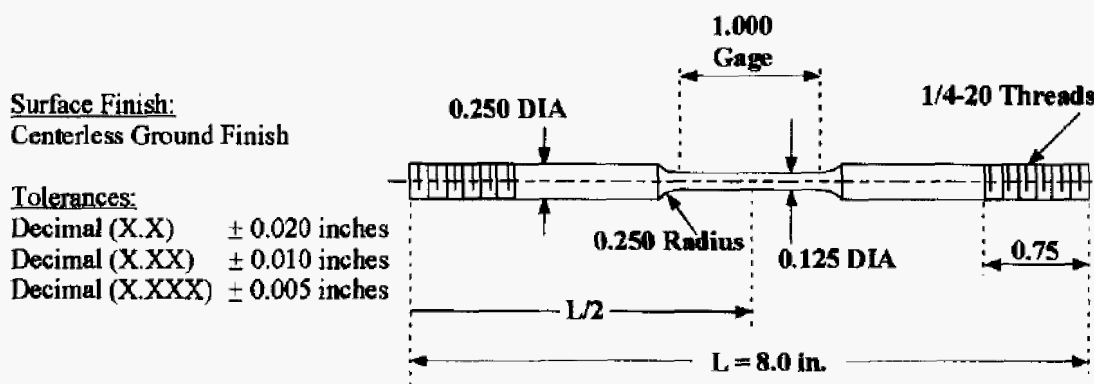


Figure 2. Engineering drawing of the SSRT specimen (units in inches)

RPP-RPT-31932, Rev. 0

Hanford Tanks AY-102 and AP-101: Corrosion and Stress Corrosion Cracking

Interim Report

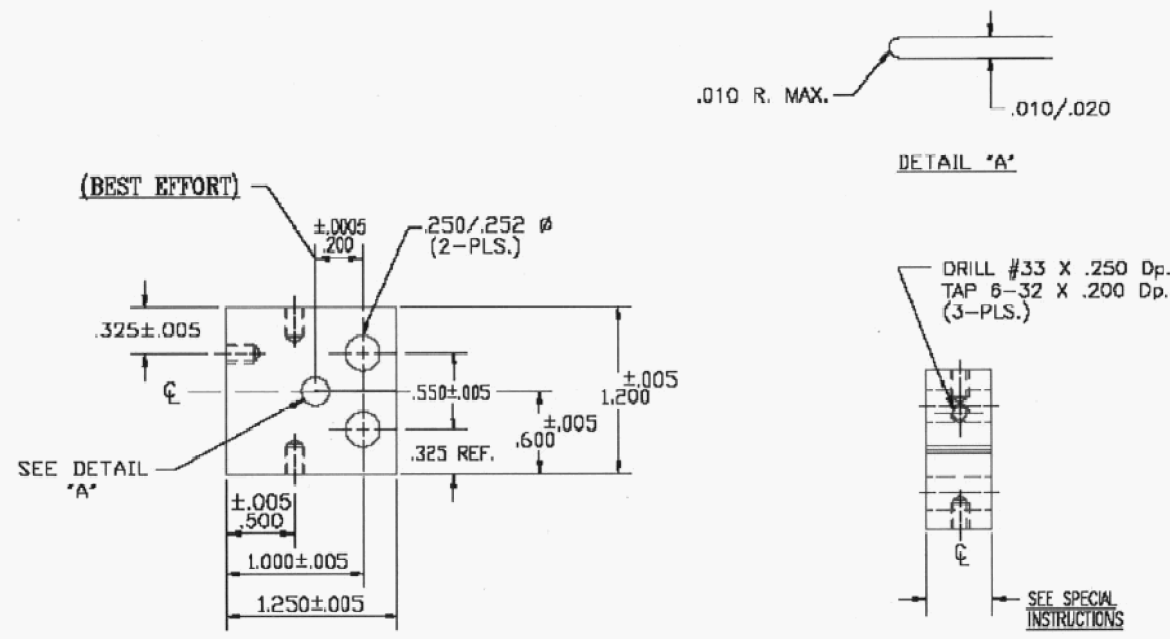


Figure 3. Engineering drawing of the CGR specimen (units in inches)

Chemicals and Solutions

Table 1 and Table 2 list the chemicals that were used to mix the standard base AY-102 and AP-101 solutions, respectively. The two solutions are considered chemically stable, and did not require continuous shaking, as was done with the previously tested AN107 solutions. The pH of the solution was adjusted after initial mixing using either sodium hydroxide or nitric acid depending on the desired final pH. Upon mixing, AY-102 solutions were typically pH ~11.7 before adjustment, whereas AP-101 solutions were typically pH > 14, due to the high initial hydroxide content.

The original plan included tests in AP-101 at pH 11. This was to allow comparisons to the previously studied AN-107 and AN-102 chemistries, many of which were tested at pH 11. However, problems were identified when adjusting AP-101 solution to pH 11. Because a considerable amount of NaOH is used in the base AP-101 simulant, the solution had pH higher than 14 requiring a significant amount of acid to achieve pH 11. Thus, to achieve a pH near 11, a considerable volume of acid would be required which would then result in a significant change in simulant chemistry. Other measures, such as CO₂ purging, might be able to get to the target pH 11 according the recommendations provided by CHM2HILL. However, the possible formation of precipitates from chemicals such as NaAlO₂ during pH adjustment may cause significant changes in the simulant chemistry.

To overcome these difficulties and still obtain an AP-101 solution with pH 11, a solution was prepared without adding both NaOH and NaAlO₂. It was found that after all other chemicals were dissolved and the solution was adjusted to the desired volume, the

RPP-RPT-31932, Rev. 0

Hanford Tanks AY-102 and AP-101: Corrosion and Stress Corrosion Cracking

Interim Report

solution pH was 11.5. The pH increased to 12.6 after dissolving the required amount of sodium aluminate. Therefore, it seems that no NaOH and sodium aluminate should be used to prepare AP-101 solution to achieve pH 11 relatively easily, which will lead to a different chemistry from the desired simulant.

Coupled with these experiments were a series of discussions in which it was intimated that AP-101 would likely never get to pH 11 because the reactions taking place in the tank tends to maintain a higher pH. Thus, it is uncertain whether any benefit could be gained by running tests in AP-101 at pH 11. As a result, only two CPP tests and three SSRTs were performed in AP-101 and they were conducted in the solutions with pH 14+.

Table 1: the list of chemicals used in the standard AY-102 solution*

Compound	Formula	Mass Required (g)
Sodium Aluminate, 2-Hydrate	NaAlO ₂ ·2H ₂ O	0.96
Sodium Carbonate	Na ₂ CO ₃	432
Sodium Oxylate	Na ₂ C ₂ O ₄	17.6
Potassium Carbonate	K ₂ CO ₃	4.8
Sodium Nitrate	NaNO ₃	0.68
Sodium Nitrite	NaNO ₂	0.28
Sodium Sulfate	NaSO ₄	10.4
Sodium phosphate , 12-Hydrate	Na ₃ PO ₄ ·12H ₂ O·¼H ₂ O	18.8
Sodium Chloride	NaCl	0.92
Sodium Fluoride	NaF	0.52
Sodium Acetate, 3-Hydrate	NaC ₂ H ₃ O ₂ ·3H ₂ O	11.2

Table 2: the list of chemicals used in the standard AP-101 solution*

Compound	Formula	Mass Required (g)
Sodium Aluminate, 2-Hydrate	NaAlO ₂ ·2H ₂ O	146.4
Sodium Hydroxide	NaOH	417.6
Sodium Carbonate	Na ₂ CO ₃	199.2
Sodium Oxylate	Na ₂ C ₂ O ₄	5.2
Potassium Nitrate	KNO ₃	335.6
Sodium Nitrate	NaNO ₃	442
Sodium Nitrite	NaNO ₂	270.4
Sodium Sulfate	NaSO ₄	16.4
Sodium phosphate , 12-Hydrate	Na ₃ PO ₄ ·12H ₂ O·¼H ₂ O	12.4
Sodium Chloride	NaCl	11.6
Sodium Fluoride	NaF	15.2
Sodium Acetate, 3-Hydrate	NaC ₂ H ₃ O ₂ ·3H ₂ O	46.4

* The chemical weight in the table is for preparing of 4L solution;

Open Circuit Potential Monitoring and Cyclic Potentiodynamic Polarization Testing

The cyclic potentiodynamic polarization (CPP) testing was performed according to ASTM G61.²

Prior to CPP testing, the specimens were ultrasonically cleaned with isopropanol for five minutes, rinsed with deionized (DI) water, and then dried with nitrogen. Note that the surface finish of these specimens is nominally equivalent to a 600 grit polish. For each test, the solution was purged with gas (nitrogen or oxygen) for one hour while waiting for the temperature to reach 50 or 77 °C (122 or 171°F) prior to inserting the specimen. Nitrogen purging was used to maintain a deaerated condition such that the oxygen reduction reaction was minimized or eliminated. Thus, under deaerated conditions the cathodic reactions could only be from other reducible species in the solution (i.e., nitrite, nitrate) or through water reduction (if the potential was negative enough). To evaluate the effect of a moderately oxidizing condition, pure oxygen gas was also purged in some cases. These tests are intended to partially mimic the conditions that might develop due to radiolysis of water to produce peroxide without the experimental complications associated with peroxide decomposition. Other tests were performed under quiescent (no gas purging) conditions. Prior to CPP testing, the open circuit potential (OCP) was monitored for 18 hours. Then the potential scan was started from -500mV vs. saturated calomel reference electrode (SCE) with a scan rate of 0.17mV/s. The scan was reversed at 1V vs. SCE or when the current reached 1mA/cm², whichever occurred first.

When a CPP test was completed, the specimen was removed from the test solution, rinsed with DI water, and then dried with nitrogen. If excessive corrosion products were present on the specimen surface, the specimen was also ultrasonically cleaned in acetone for five minutes and rinsed with DI water and dried with nitrogen. The post-test appearance of the specimen was photographically documented to show any evidence of corrosion attack. Finally, the tested specimens were stored in separate specimen bags in a desiccator for any other further possible analysis.

Slow Strain Rate Testing

SSR testing was performed according to the guidelines provided in ASTM G129³ using cylindrical tensile specimens at a constant extension rate of 10⁻⁶ in/in-s (unless otherwise noted). To perform the tests, the specimen was placed into a Teflon test cell and the load applied using pull rods that entered the cell through sliding seals. After

² "Standard Test Method for Conducting Cyclic Potentiodynamic Polarization Measurements for Localized Corrosion Susceptibility of Iron-, Nickel-, or Cobalt-Based Alloys", ASTM G61

³ "Standard Practice for Slow Strain Rate Testing to Evaluate the Susceptibility of Metallic Materials to Environmentally Assisted Cracking", ASTM International (2005).

RPP-RPT-31932, Rev. 0

Hanford Tanks AY-102 and AP-101: Corrosion and Stress Corrosion Cracking

Interim Report

insertion of the specimen and pull rods into the load frame, the solution of interest was introduced and heated to either 50 or 77°C. Tests were either conducted at open circuit or at an applied potential against a reference electrode (SCE) maintained at room temperature using a Luggin probe/salt bridge that was filled with the test solution. A platinum flag was used as a counter electrode. All SSRT experiments were performed under quiescent conditions.

Post-test analysis consisted of stereographic optical examination at 10 – 63x. Analyses using higher magnification optical microscopy, metallographic cross sectional analysis, and scanning electron microscopy (SEM) can be used on an as-needed basis. In previous work where evidence of SCC was present, metallographic cross sectional analysis was utilized to estimate a crack growth rate by dividing the maximum crack length observed by the time to failure (total test time). For the purposes of semi-quantitatively comparing the SSRT results, the estimated crack growth rate (CGR) was divided into the following classifications:

<u>Degree of SCC</u>	<u>Estimated CGR (mm/s)</u>	<u>Estimated CGR (in/s)</u>
Major	$\geq 3 \times 10^{-6}$	$\geq 1.2 \times 10^{-7}$
Moderate	$3 \times 10^{-6} - 5 \times 10^{-7}$	$1.2 \times 10^{-7} - 2 \times 10^{-9}$
Minor	$\leq 5 \times 10^{-7}$	$\leq 2 \times 10^{-9}$
None	No indications of SCC	

Note that the crack growth rates determined from the SSR tests should be used with caution and only for comparative purposes. Furthermore, the crack growth rates estimated from the SSR test results should not be compared with rates determined in future constant load crack growth rate tests using compact tension specimens. The SSRT CGRs tend to be higher because of the imposed continued straining of the specimens; a condition unrealistic for storage tanks.

The time-to-failure and the strain at failure of the specimens did not always reflect clearly if SCC was present. Also, the degree of SCC was not easily established from these parameters. Therefore, the occurrence of SCC was always confirmed by visual inspection, and the severity of SCC was determined from the estimated crack growth rate as described above.

RPP-RPT-31932, Rev. 0

Hanford Tanks AY-102 and AP-101: Corrosion and Stress Corrosion Cracking

Interim Report

RESULTS AND DISCUSSION

Electrochemical Polarization Behavior

This section summarizes the results and key findings from the electrochemical tests (i.e., OCP, CPP tests). The effects of pH, temperature and oxygen content in the solution are discussed. Table 3 summarizes the completed tests for this phase of the work.

Table 3: CPP tests completed during Phase 1

Test ID	Solution Chemistry	pH	Temp. (°C)	Gas Purge	Sample	OCP (mV vs. SCE)	Comments
CPP 1	AY-102	11	50	Nitrogen	Steel	-901	No visible pitting
CPP 2	AY-102	11	77	Nitrogen	Steel	-942	No visible pitting
CPP 3	AY-102	11	50	Nitrogen	Platinum	-206	No visible pitting
CPP 4	AY-102	11	77	Nitrogen	Platinum	-146	No visible pitting
CPP 5	AP-101	14+	50	Nitrogen	Steel	-851	No visible pitting
CPP 6	AP-101	14+	77	Nitrogen	Steel	-638	No visible pitting
CPP 7	AY-102	11	50	Quiescent	Steel	-228	No visible pitting
CPP 8	AY-102	11	77	Quiescent	Steel	-225	No visible pitting
CPP 9	AY-102	11	50	Oxygen	Steel	-204	No visible pitting
CPP 10	AY-102	11	77	Oxygen	Steel	-234	No visible pitting

The samples initially experienced active dissolution and then reached a pseudo-passive region at both 50°C and 77°C in AY-102. FIGURE 4 shows the comparison of the CPP curves in AY-102 at these two temperatures. The (pseudo) passive current densities at both temperatures were almost identical (on the order of 10^{-5} A/cm²). An additional anodic nose was observed at around -0.5 V which has not been identified as yet. At higher potentials, the curves showed a sharp increase in the current at approximately 0.6 V (vs. SCE). Furthermore, the current densities on the reversal scan were lower than that on the forward scan. The observation of a negative hysteresis indicated that the sharp increase in the current may not be resulted from pitting corrosion but is rather due to transpassive dissolution, oxidation of a species in the solution (very likely water oxidation given the pH), or a combination of the two. By way of comparison, the reversible potential for water oxidation at pH 11 at 25 °C is approximately 0.55 V vs. SCE. The absence of pits was confirmed by the inspection of the post-test samples (shown in Appendix A).

The CPP tests performed with platinum wires in AY-102 indicated an increase in the current at similar potential ranges as that was observed in Figure 4. The comparisons of the CPP curves between platinum and steel are shown in Figure 5 (a) and Figure 5 (b) for 50°C and 77°C, respectively. Clearly, the polarization curve on platinum also showed an increase in the current at similar potentials. This finding further illustrated that the

current increase was not from pitting corrosion. Rather, it is most likely due to water oxidation and possibly concomitant transpassive dissolution of the steel.

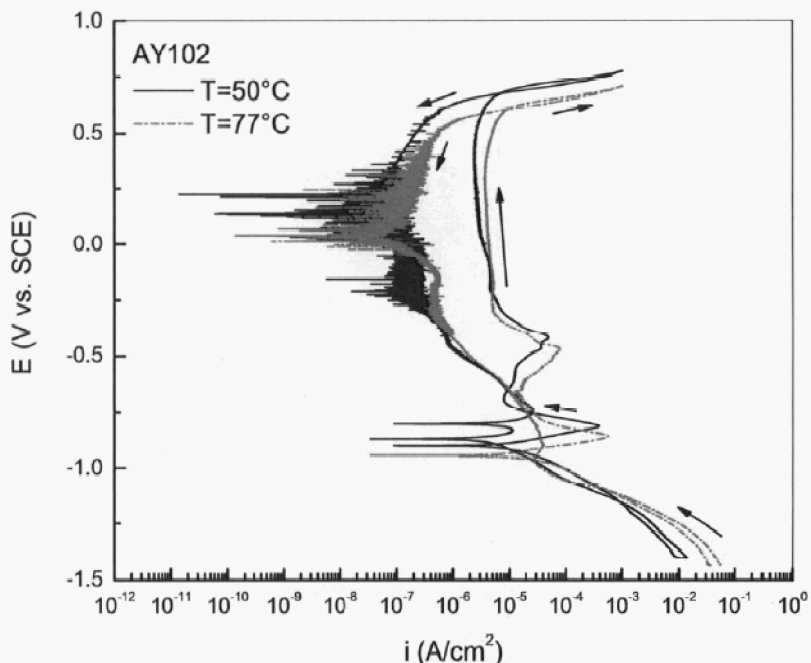
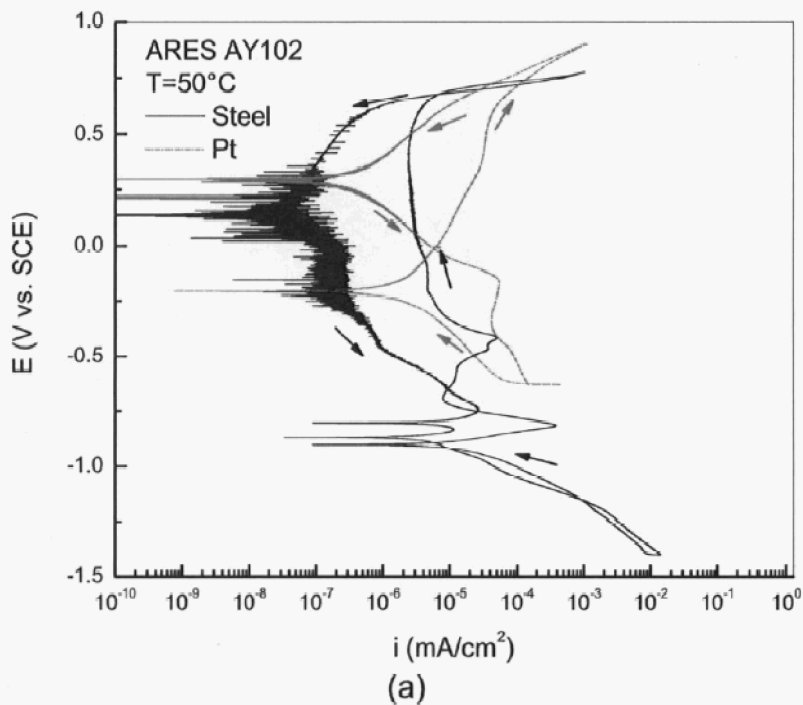


Figure 4: Comparison of CPP curves in AY-102 solution, pH 11 at 50 and 77°C.



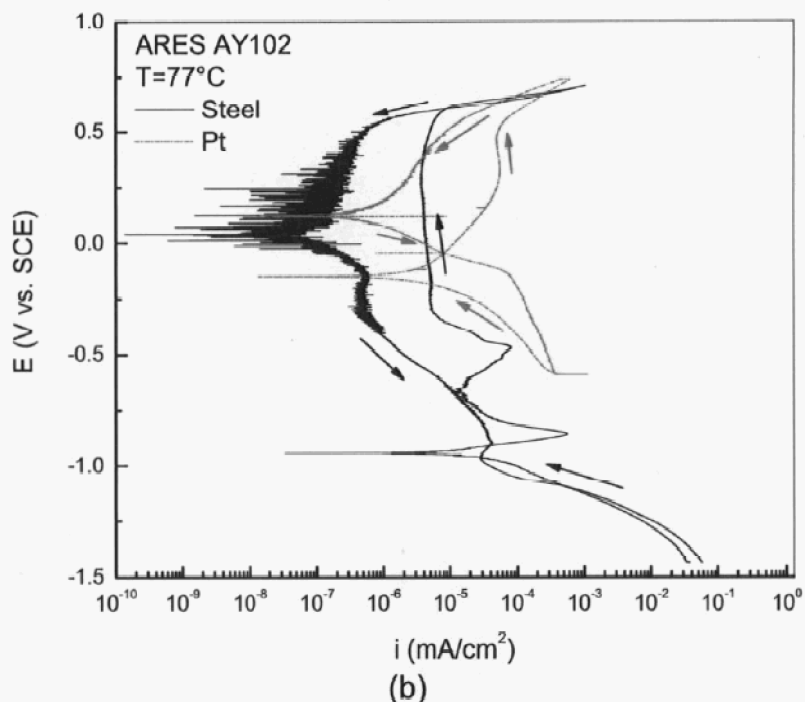


Figure 5: Comparison of CPP curves of steel and platinum in AY-102 solution, pH 11. (a) at 50°C; (b) at 77°C.

The CPP curves in AP-101 (pH > 14) at both 50 °C and 77 °C are similar to AY-102 except that no active-passive transition was observed, as shown in Figure 6. The curves exhibited a fairly wide passive region prior a current increase at approximately 0.48 V vs. SCE. Again, this current increase is most likely associated with water oxidation (reversible potential for water oxidation at pH 14 is approximately 0.44 V vs. SCE) with possible concomitant transpassive dissolution. The current densities on the reversal scan again were lower than that on the forward scan. No positive hysteresis was observed and the inspection of the samples confirmed the absence of pitting corrosion. The OCP values at both temperature levels were slightly more positive than those observed in AY-102, likely due to higher amount of nitrate concentration in this solution. The contributions of high nitrate and/or nitrite concentration to the cathodic reactions are discussed below.

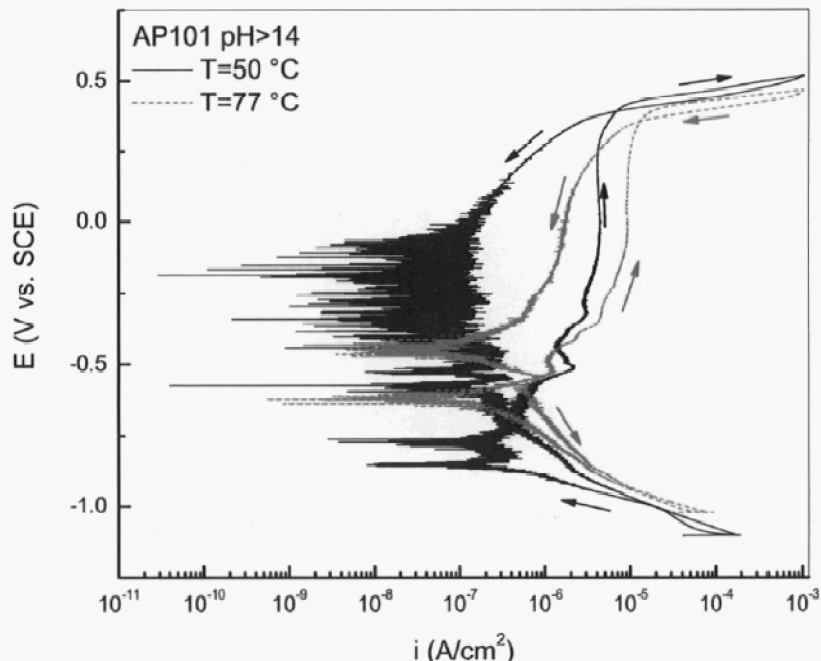


Figure 6: Comparison of CPP curves in AP-101 solution, pH > 14 at 50 and 77°C.

When the nitrite and nitrate concentrations are significant in the stimulant, the cathodic reactions could be dominated by the reduction of nitrogen species and therefore result in a positive shift of the OCP. As shown in Figure 7, the comparison of the CPP curves obtained between AN-107 simulant and AY-102 simulant showed that the OCP in AN-107 simulant was much more positive than that observed in AN-102 simulant. The comparison of the solution composition of these two solutions indicated that the combined nitrate • nitrite concentration was 4.9M in AN-107 compared to 0.003M in AY-102. At 77°C, the OCP in AP101 was approximately 300 mV more positive than in AY-102, which is in consistent with the discussion above regarding the dominated cathodic reactions since nitrate and nitrite concentration present in AP-101 are much higher (2.13M and 0.98M, respectively) compared to AY-102 simulant. The OCP in AP-101 simulant at 50°C, however, only slightly differed from that in AY-102. This seems to be unexpected considering the higher nitrate and nitrite concentrations present in AP-101. More investigation may be needed to understand the dominant cathodic kinetics at 77°C in AP-101.

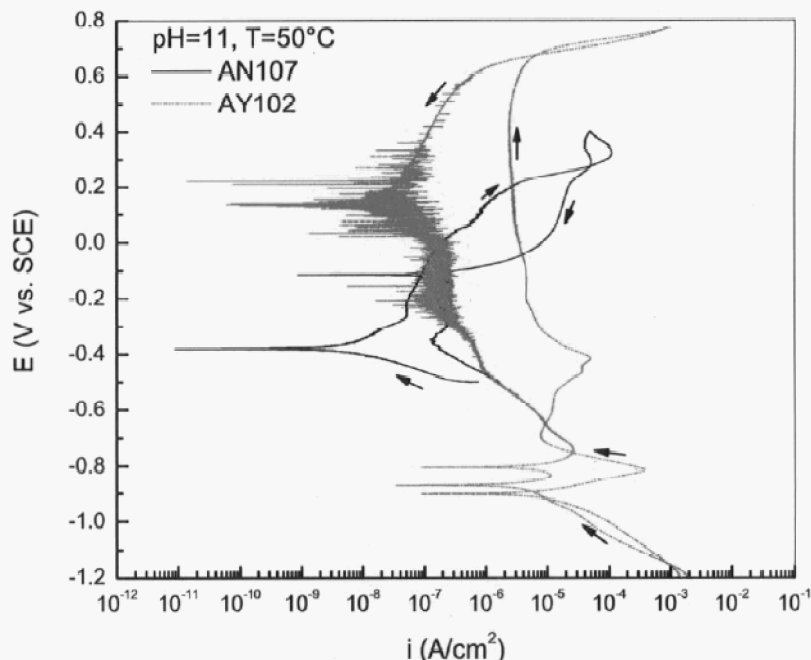
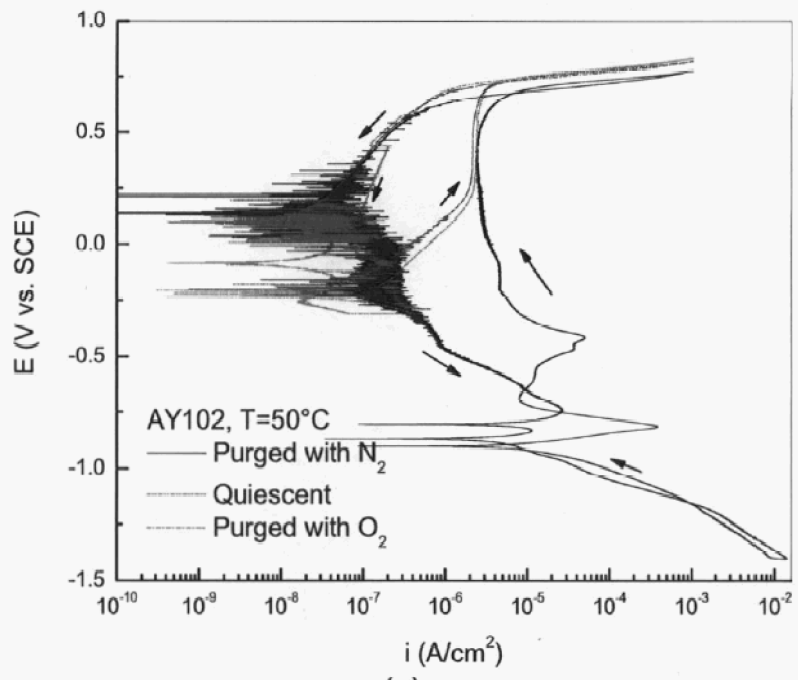


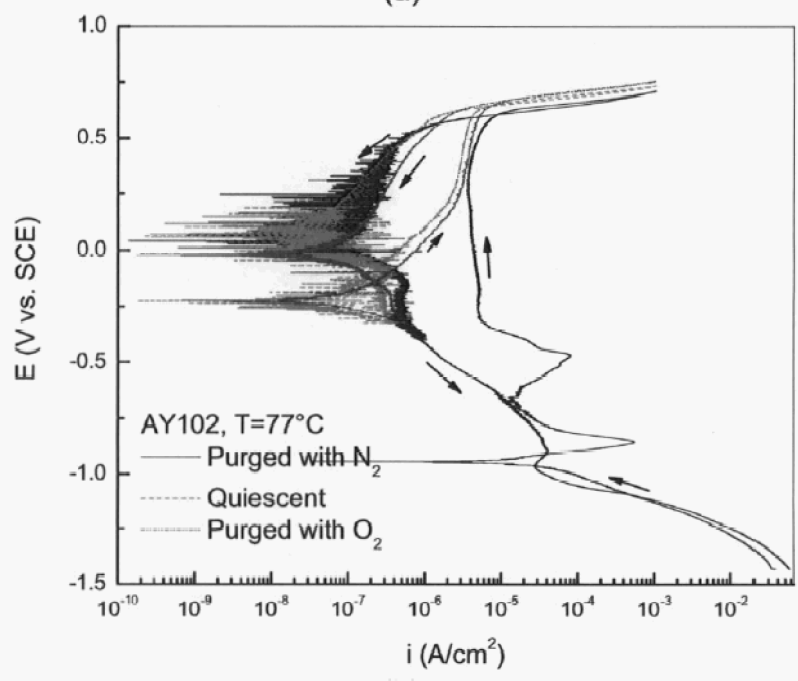
Figure 7: Comparison of CPP curves in AN102 and in AN107 simulant at pH 11 and 50°C.

The OCP of carbon steel in AY-102 is more positive in the presence of oxygen than that in the absence of oxygen. FIGURE 8 shows the comparison of the CPP curves at three different conditions for each temperature level: purged with nitrogen, quiescent, and purged with oxygen. Clearly, independent of temperature, the OCP was approximately 700 mV more positive when the solution was under quiescent conditions. There was no further change in the OCP when the solution was purged with pure oxygen at both temperatures.

The shift in the OCP was likely due to the change in the dominant cathodic reactions. In the absence of oxygen, the primary cathodic reaction in AY-102 was water reduction. However, when oxygen is present, the cathodic reaction was dominated by the oxygen reduction reaction resulting in the expected positive shift in the OCP. Again, it should be noted that oxygen content seemed to have no appreciable effect on OCP in the case of AN-107 because the presence of high nitrate and nitrite concentrations and their reduction reactions (perhaps also combined with other reduction reactions) dominated the cathodic reaction.



(a)



(b)

Figure 8: Comparison of CPP curves in AY-102 solution (pH 11) under quiescent condition, purged with nitrogen and with oxygen. (a) 50°C; (b) 77°C.

RPP-RPT-31932, Rev. 0

Hanford Tanks AY-102 and AP-101: Corrosion and Stress Corrosion Cracking

Interim Report

Summary of Electrochemical Behavior

- No pitting corrosion was observed in either AY-102 at pH 11 or AP-101 at pH 14+ even at very high potentials, and this appears independent of the testing temperature
- The CPP curves at 50°C and at 77°C in both simulants showed no appreciable differences resulting from the increase in temperature
- The OCP in AY-102 was much more negative than that observed in AN107 likely because water reduction was the dominant cathodic reaction in AY-102
- The presence of oxygen shifted the OCP in the noble (higher potential) direction in AY-102 primarily because the oxygen reduction reaction was the dominant cathodic reaction

Slow Strain Rate Testing

This section summarizes the results and key findings from the SSR tests that were performed to explore the susceptibility of AAR TC 128 Grade B tank car steel to SCC, primarily as a function of solution temperature, chemistry, and potential.

A summary of the SSRT results is shown in TABLE 4. This table includes results from both AY-102 and AP-101 solution chemistries. The table is organized based first by test environment, then by increasing temperature, and finally by decreasing potential.

Typical stress-strain curves are shown in Figure 9 and Figure 10 for the tests conducted in AY-102 and they are grouped based on test temperature and applied potential.

Table 4: Summary of SSRT results from the 2007 test series.

Solution Chemistry	pH	Temp. (°C)	Applied Potential (mV vs. SCE)	Failure Strain (%)	Failure Time (hrs)	Visual	Test ID
				Air			
Air	-	77	-	23.3	64.5	No visible SCC	SSR 4
				AY-102			
AY-102	11	50	0	23.2	64.3	No visible SCC	SSR 2
AY-102	11	50	-750	25.1	71.8	No visible SCC	SSR 8
AY-102	11	50	-775	24.3	64.3	Negligible	SSR12
AY-102	11	50	-800	22.7	62.1	Negligible	SSR13
AY-102	11	77	0	21.0	59.4	Minor cracking	SSR 3
AY-102	11	77	-330 (OCP)	24.9	67.6	No visible SCC	SSR 1
AY-102	11	77	-750	25.7	73.3	Negligible	SSR 9
AY-102	11	77	-775	23.1	64.2	Minor cracking	SSR10
AY-102	11	77	-800	21.1	61.4	Minor cracking	SSR11
				AP-101			
AP-101	14+	50	0	22.8	65.1	Minor cracking	SSR 6
AP-101	14+	77	0	25.3	67.9	Negligible	SSR 7
AP-101	14+	77	-448 (OCP)	22.5	63.8	No visible SCC	SSR 5

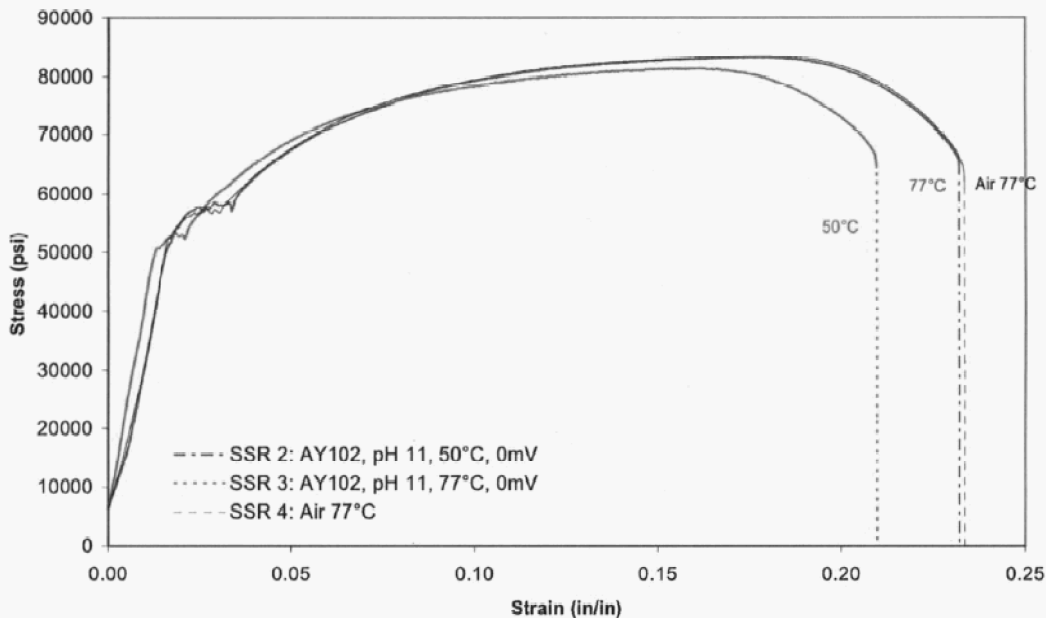


Figure 9: Stress-strain SSRT results comparison in AY-102 at two temperatures.

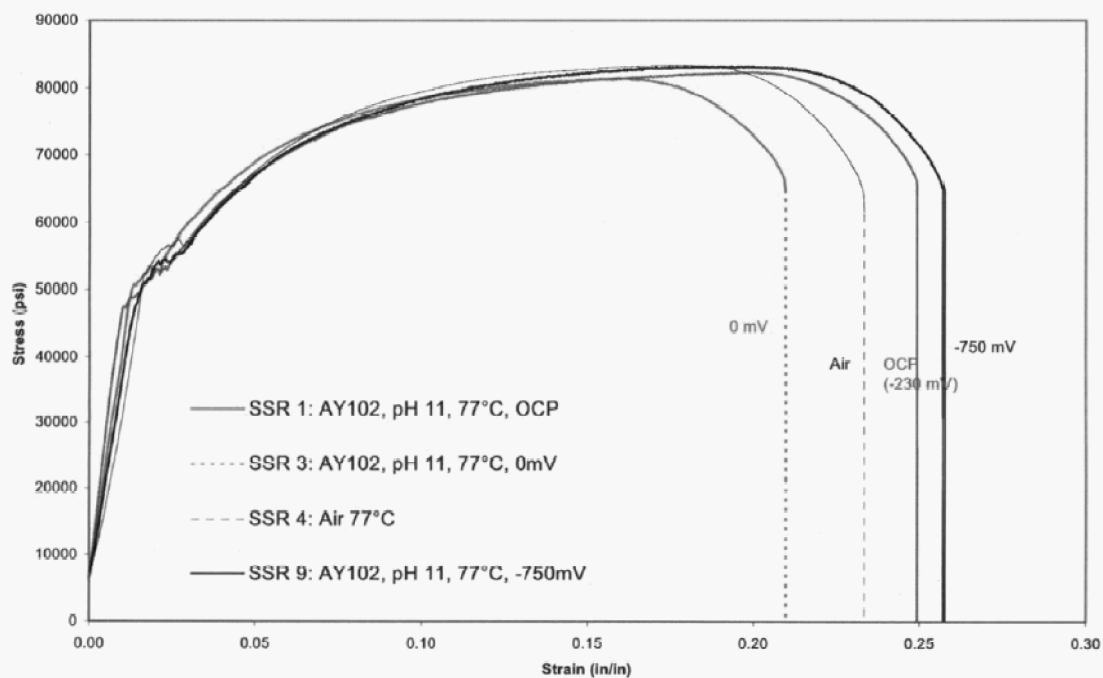


Figure 10: Stress-strain SSRT results comparison in AY-102 at different applied potentials

RPP-RPT-31932, Rev. 0

Hanford Tanks AY-102 and AP-101: Corrosion and Stress Corrosion CrackingInterim Report

From Figure 9 and Figure 10, it seems that in AY-102 simulant, temperature and the applied potential do not have a significant impact on the failure strain, which varied slightly from 21.0% to 25.7% for all samples and is consistent with the failure strain measured in air. Observations in AY-102 also did not indicate any identifiable trends with respect to temperature and potential on failure strain based on the tests conducted thus far.

Temperature slightly influenced the severity of cracking, in terms of failure time and the cracking ranking by visual observation after testing, as shown in Table 4. In AY-102 simulant at 0 mV vs. SCE, SCC was not observed at 50°C, whereas minor cracking was noted at 77°C. Thus, increasing the temperature from 50°C to 77°C at the same applied potential appeared to slightly increase the susceptibility of carbon steel to SCC. In the AP-101 simulant at the same conditions, however, SCC was observed at both temperatures with slightly more severe cracking noted at 50°C compared to 77 °C. Therefore, the increase in the temperature seemed to reduce the susceptibility of SCC based on the obtained results. More tests may be needed to verify this finding.

The CPP testing has demonstrated that carbon steel in both AY-102 and AP-101 at the temperature and pH levels investigated was not susceptible to pitting corrosion. The polarization behavior in AY-102 did show evidence of an active-passive transition at approximately -800 mV vs. SCE. It is well known that SCC could occur in this potential range in carbonate solutions that are somewhat similar to the AY-102 simulant. To investigate the susceptibility of carbon steel in this potential range, a set of SSR tests was performed with the potential controlled at -750 mV, -775 mV, and -800 mV vs. SCE at both 50°C and 77°C in AY-102.

The potential applied to the samples during SSR testing appeared to affect to susceptibility to SCC to some extent, although failure strain remained comparable to other conditions and failure time only exhibited a slight change. For example, in AY-102 at 77°C, cracking was observed at 0 mV and potentials below (more negative) -750 mV vs. SCE. Based on a limited number of tests conducted at potentials between 0 mV and -750 mV, however, no cracking or only negligible cracking has been observed thus far. The failure time increased from 59.6 hrs to 73.3 hrs when reducing the applied potential from 0 mV to -750mV which then subsequently decreased to ~60 hrs when the potential was further reduced to -800 mV. The failure strain did not change considerably when changing applied potential from 0 mV to -800 mV vs. SCE.

The nitrite/nitrate ratio effect on cracking as a function of applied potential was plotted and overlapped with the figure developed from research conducted for AN-107, as shown in Figure 11. It can be seen that SCC was observed at -800 mV vs. SCE in the AY-102 simulant, although the nitrite/nitrate ratio was 0.5. This seems to be in contradiction with that was observed in AN-102. However, it should be noted that nitrite concentration is 0.001M, which is significantly lower than the critical nitrite concentration noted to provide (at least some) SCC inhibition in AN-107 simulant (~1.2M). Thus, even though the same nitrite/nitrate ratio was present, SCC was still observed perhaps because there was insufficient inhibitor present, assuming nitrite still plays important

role in the AY-102 simulant. This then may suggest that high nitrite/nitrate ratio is beneficial only when the nitrite concentration is above the critical inhibition level.

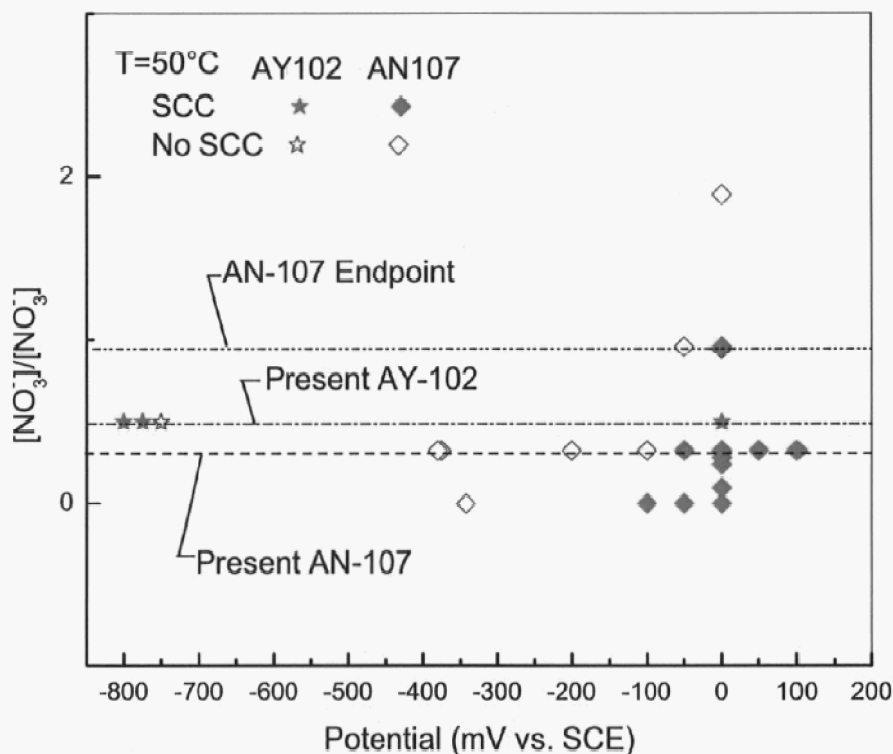


Figure 11: Effect of nitrite/nitrate concentration ration on the propensity for SCC in AN-107 simulant and AY-102 simulant.

The applied potential seemed to affect the propensity for SCC in the AY-102 simulant differently at 50°C and 77°C. The observed extent of cracking as a function of applied potential is shown in Figure 12. Note the ranking of the cracking degree was based on a subjective visual inspection of the tested samples. The calculation of crack growth rate will be conducted but will not be presented in this Phase 1 report. At 50°C, cracking was not observed at potentials equal to or above -750 mV vs. SCE. At 77°C, however, it seems there is an immune potential region to cracking between 0 and -750 mV vs. SCE, outside of which cracking may be possible. At both temperatures, cracking appeared to be possible at potentials close to the active-passive transition potential.

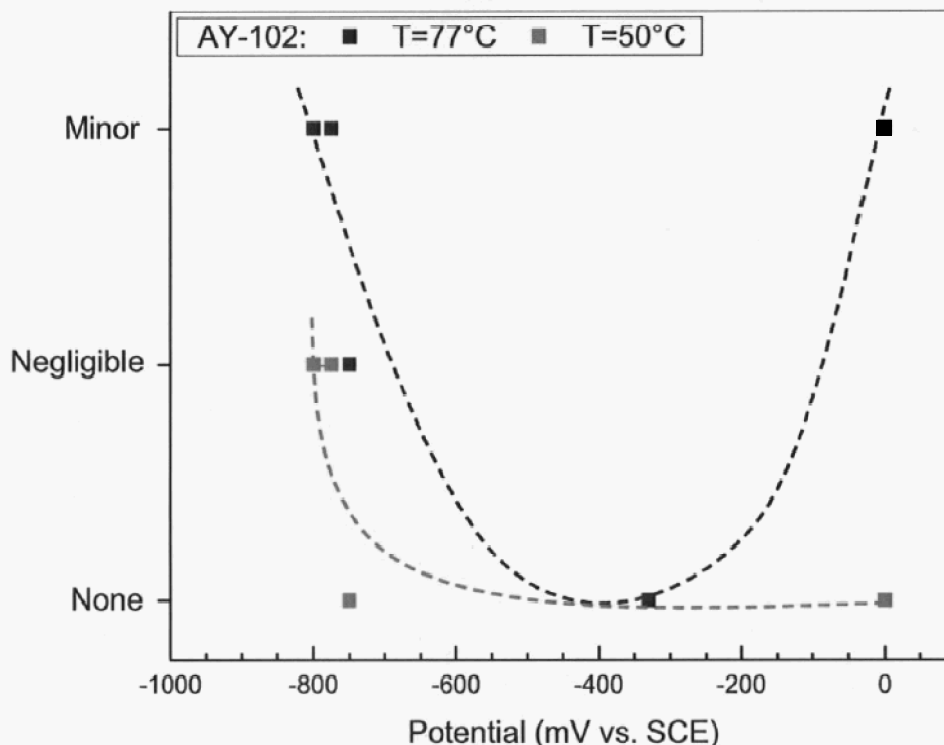


Figure 12: The effect of applied potential on the propensity for SCC in AY-102 simulant at 50°C and 77°C

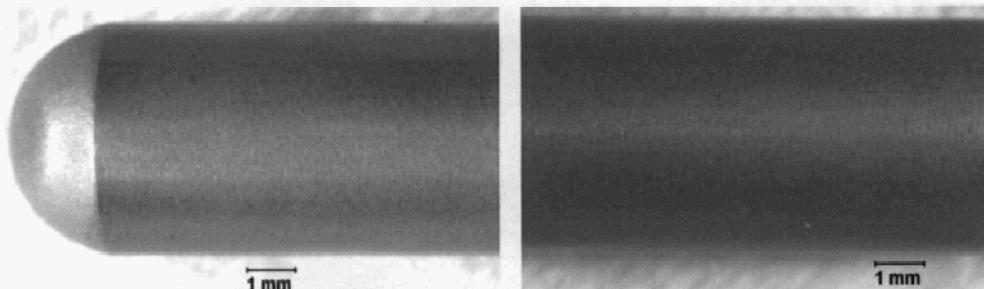
Summary of SSRT Testing

- Increasing the temperature from 50°C to 77°C did not appreciably change the susceptibility to SCC in AY-102, but slightly increased cracking susceptibility in AP-101 at 77°C
- SCC seemed to be relatively minor in both AY-102 and AP-101 and no severe cracking has been observed in the pH range and the applied potential range being evaluated
- Cracking appeared to be slightly worse at 0 mV and at potentials below the active-passive transition potential observed on CPP curves in AY-102 at 77°C (i.e. the “nose” potential); at 50°C, cracking was only observed at potentials more negative than -750 mV

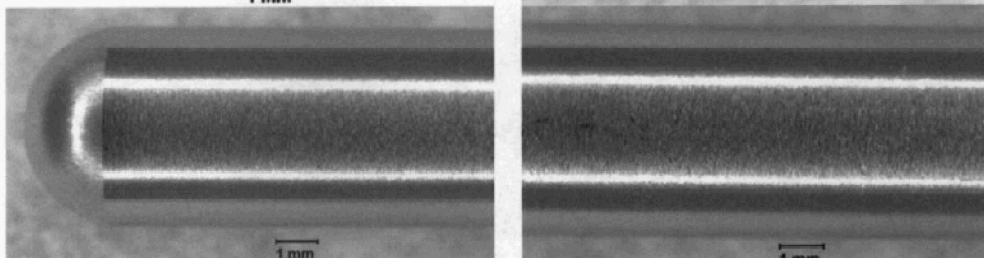
APPENDIX A

Photographs of Cyclic Potentiodynamic Polarization Test Specimens

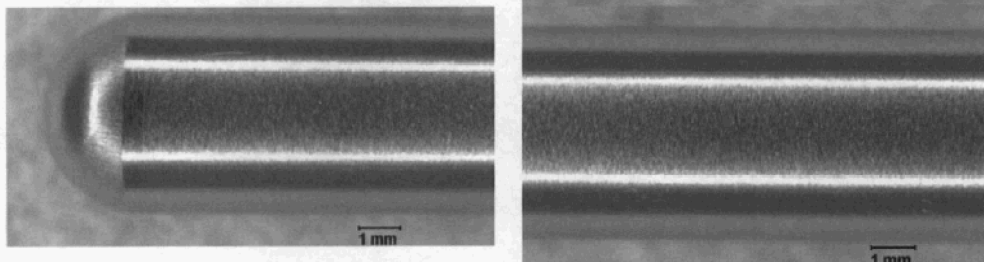
AY-102 pH=11
T=50°C
Purged with N₂



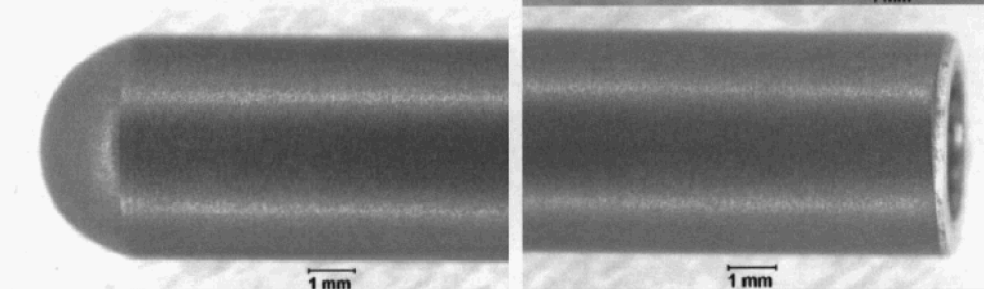
AY-102
pH=11 T=50°C
Quiescent
condition



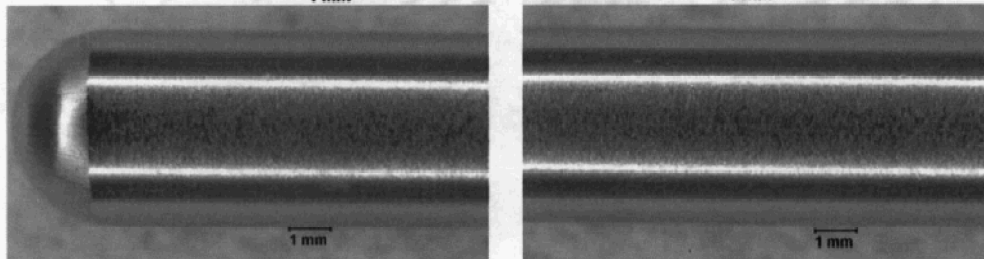
AY-102
pH=11 T=50°C
Purged with O₂



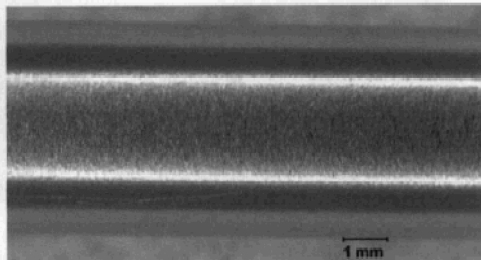
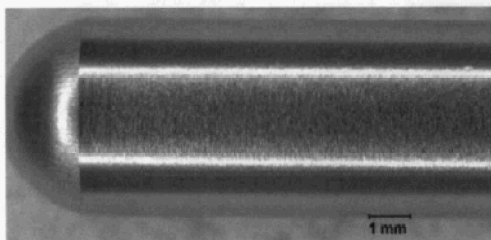
AY-102 pH=11
T=77°C
Purged with N₂



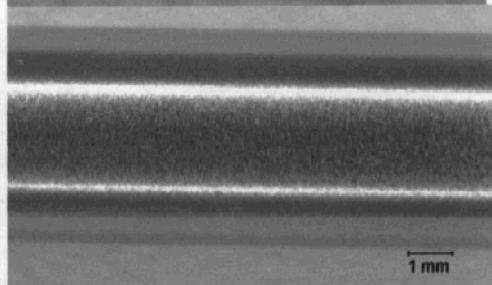
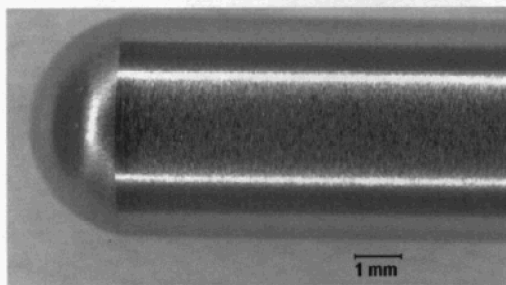
AY-102
pH=11 T=77°C
Quiescent
condition



AY-102
pH=11 T=77°C
Purged with O₂



AP-101 pH=11
T=50°C



AP-101
pH=11 T=77°C

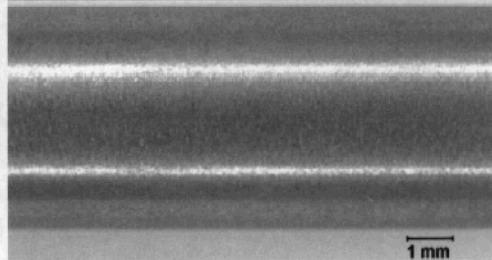
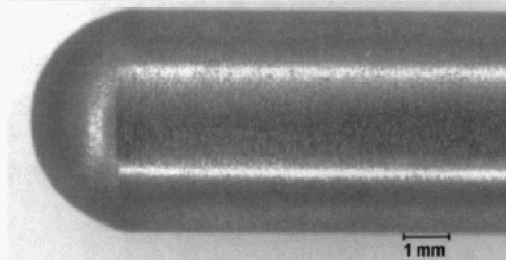


Figure 13: The appearance of samples after CPP tests.

APPENDIX B

Photographs of Slow Strain Rate Test Specimens

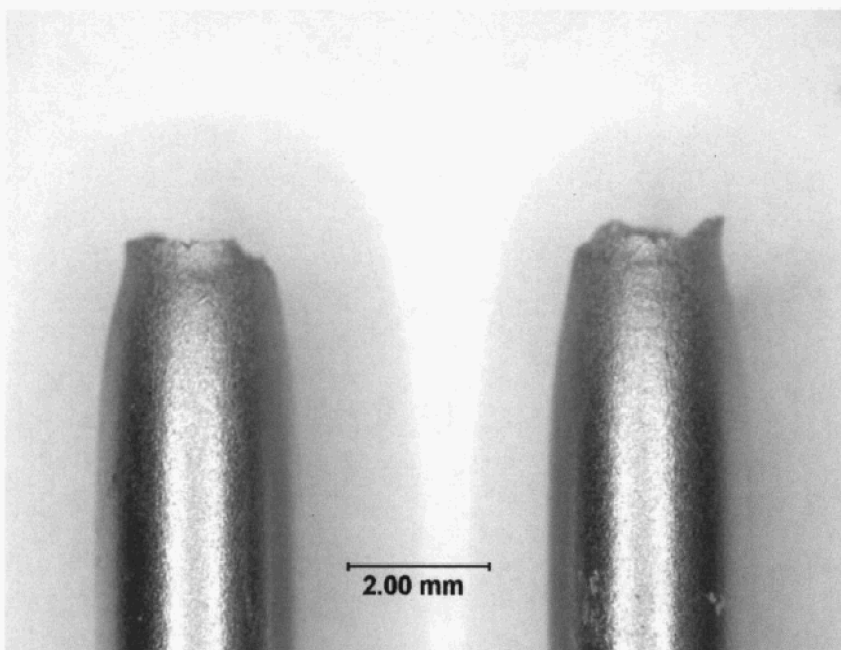


Figure 14: A stereo-micrograph of the sample from SSR 1: AY-102, pH 11, 77°C at OCP

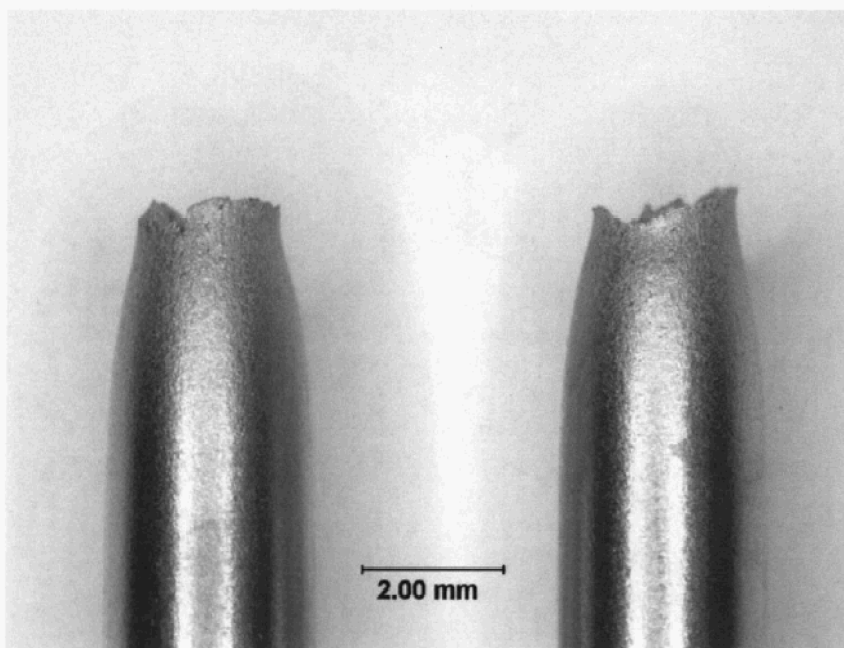


Figure 15: A stereo-micrograph of the sample from SSR 2: AY-102, pH 11, 50°C at 0 mV vs SCE.

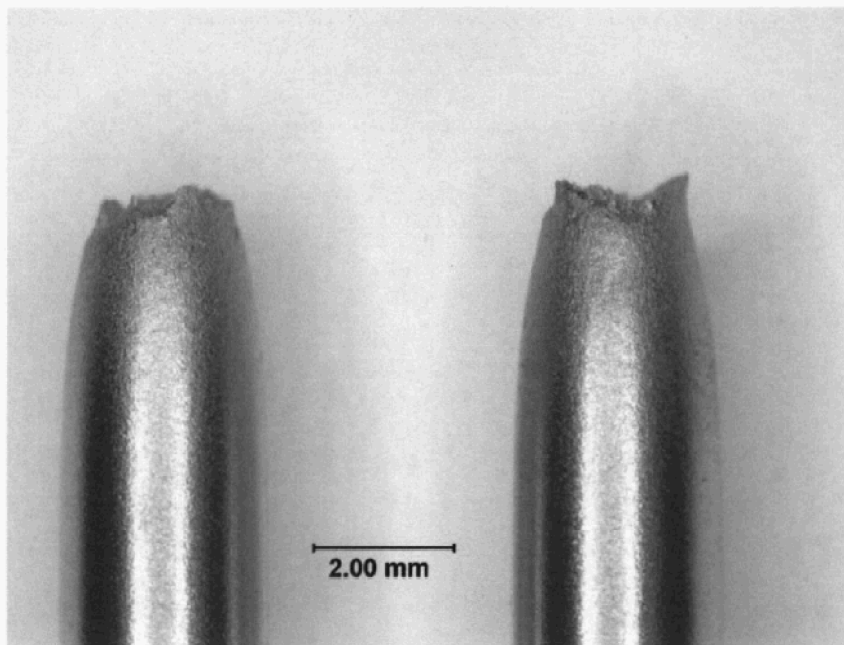


Figure 16: A stereo-micrograph of the sample from SSR 3: AY-102, pH 11, 77°C at 0 mV VS SCE.

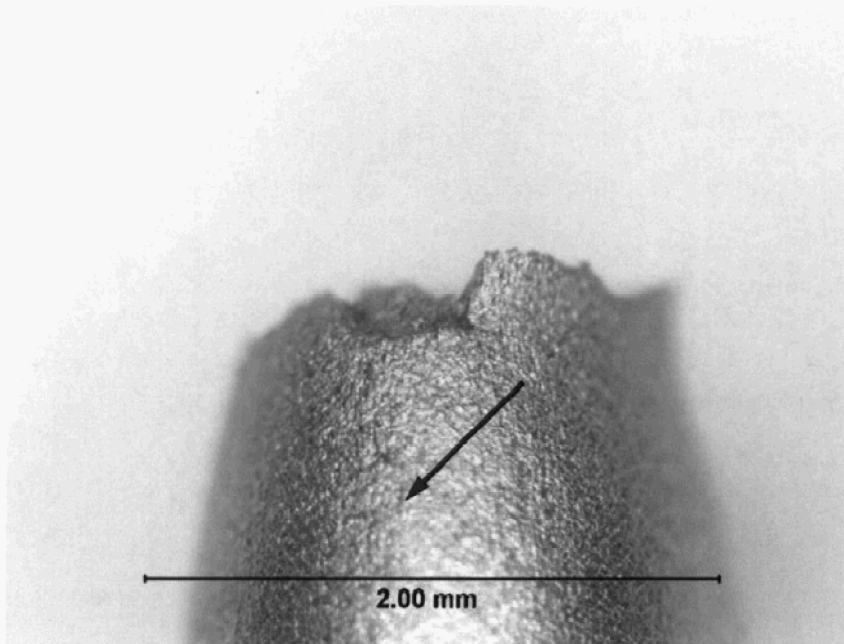


Figure 17: A stereo-micrograph of the sample from SSR 3: AY-102, pH 11, 77°C at 0 mV VS SCE. Note the minute crack near the fracture surface, as indicated by the black arrow.

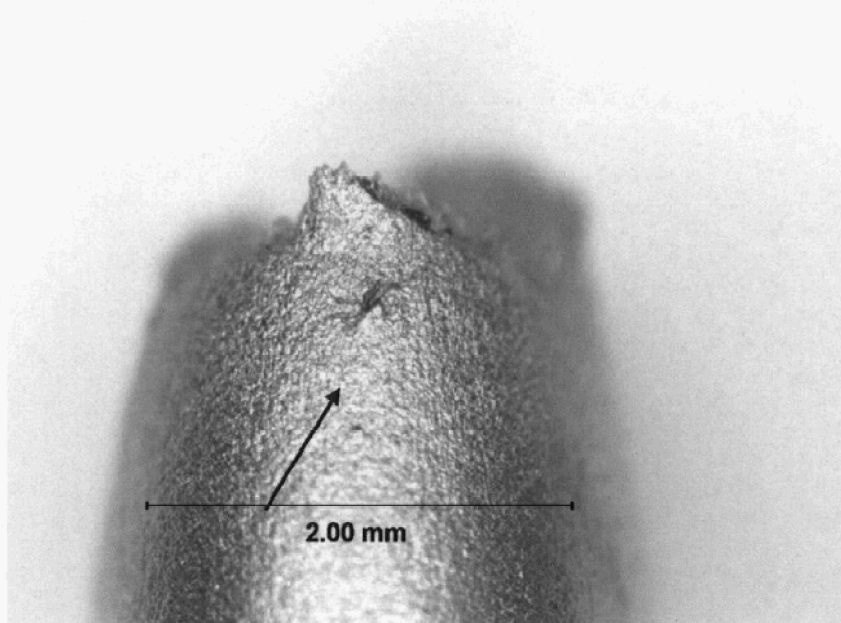


Figure 18: A stereo-micrograph of the sample from SSR 3: AY-102, pH 11, 77°C at 0 mV vs SCE. Note the crack near the fracture surface, as indicated by the black arrow.

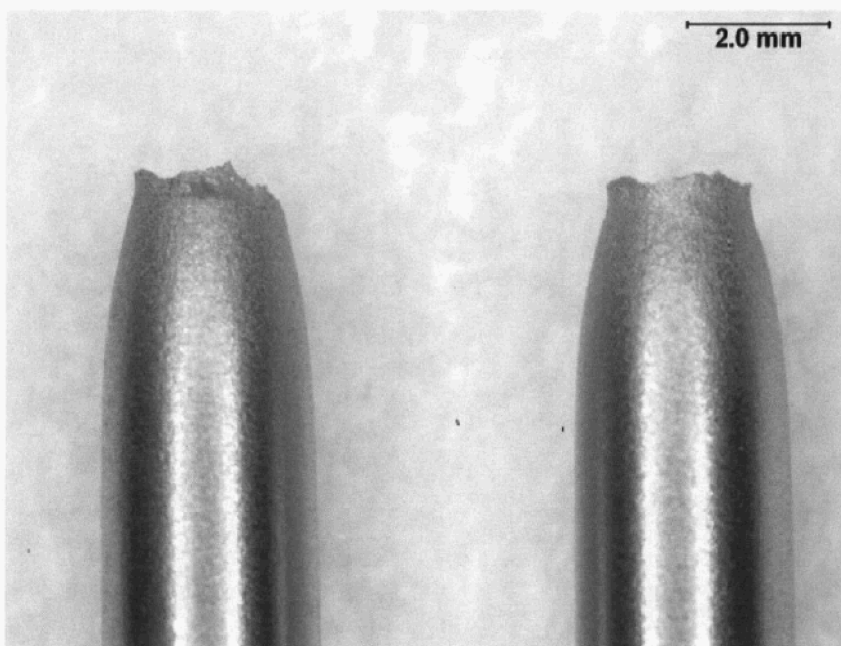


Figure 19 A stereo-micrograph of the sample from SSR 4 in air.

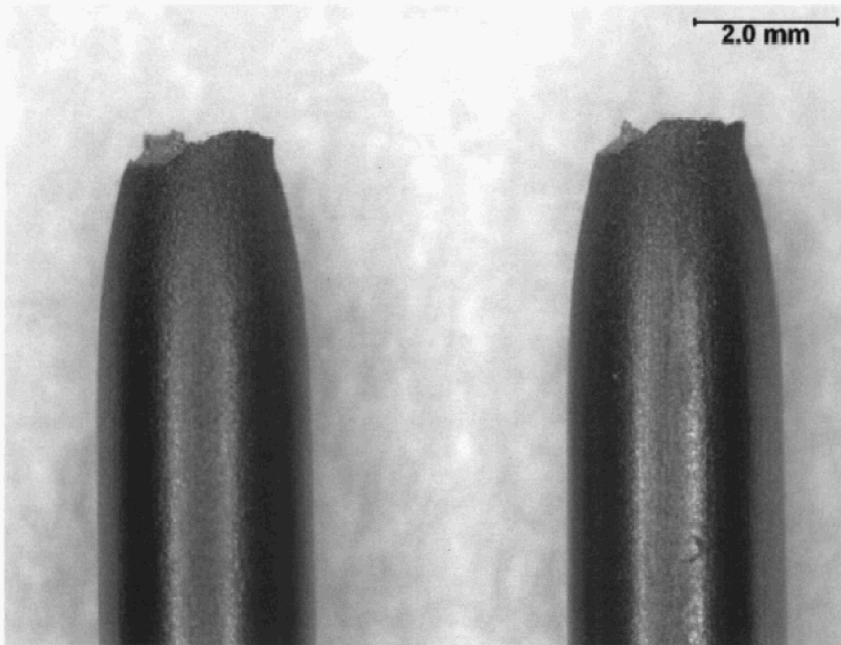


Figure 20: A stereo-micrograph of the sample from SSR 5: AP-101, pH 14+, 77°C at OCP

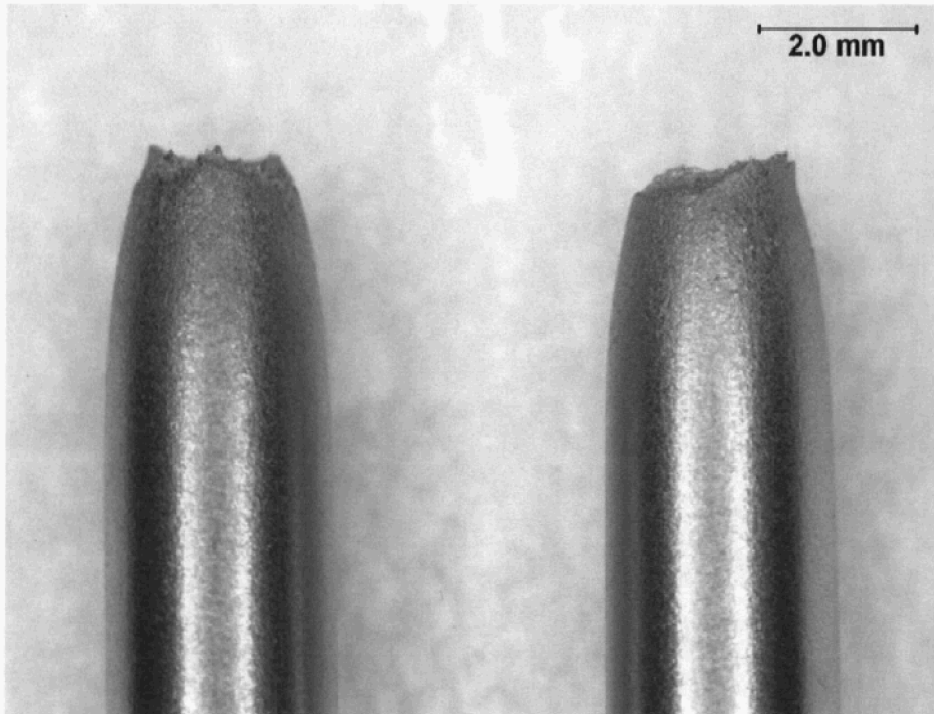


Figure 21: A stereo-micrograph of the sample from SSR 6: AP-101, pH 14+, 50°C at 0 mV vs SCE.

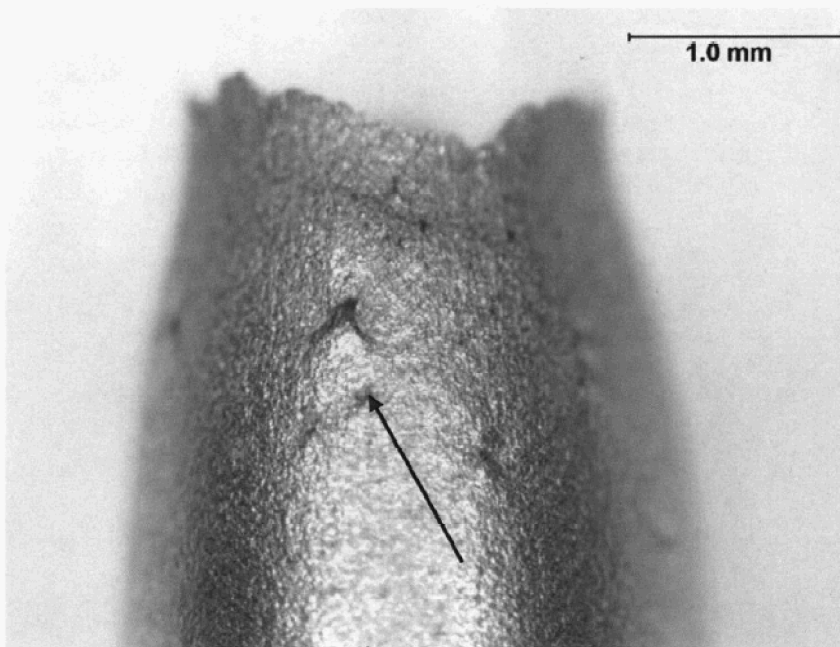


Figure 22: A stereo-micrograph of the sample from SSR 6: AP-101, pH 14+, 50°C at 0 mV vs SCE (magnified). Note the crack, as indicated by the black arrow

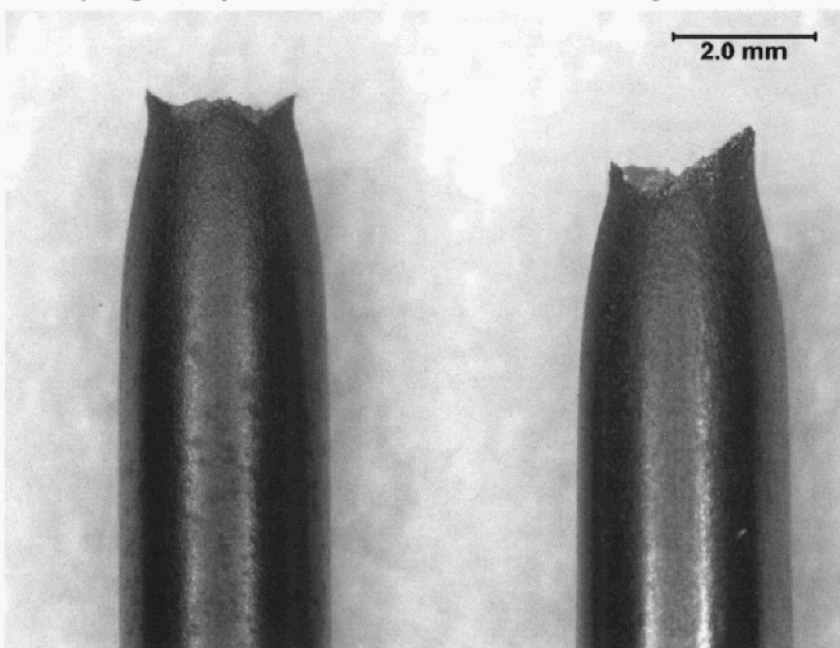


Figure 23: A stereo-micrograph of the sample from SSR 7: AP-101, pH 14+, 77°C at 0 mV vs SCE.

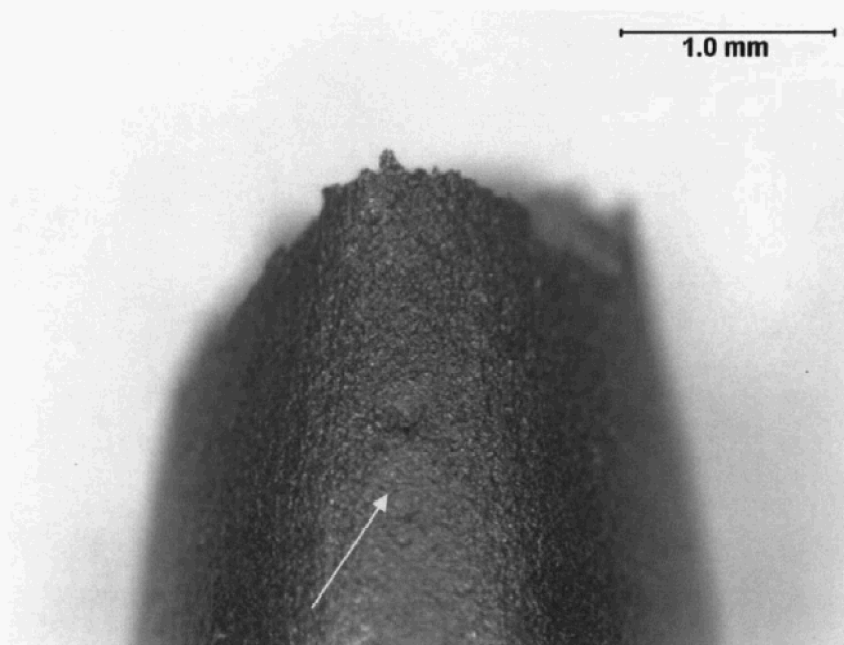


Figure 24: A stereo-micrograph of the sample from SSR 7: AP-101, pH 14+, 77°C at 0 mV vs SCE (magnified). Note the crack, as indicated by the white arrow.

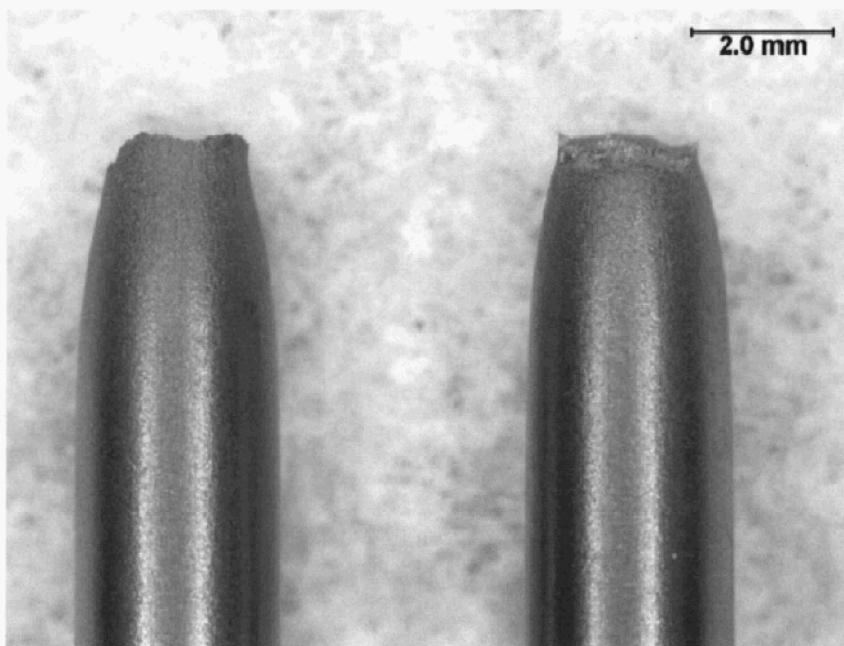


Figure 25: A stereo-micrograph of the sample from SSR 8: AY-102, pH 11, 50°C with applied potential of -750 mV vs SCE.

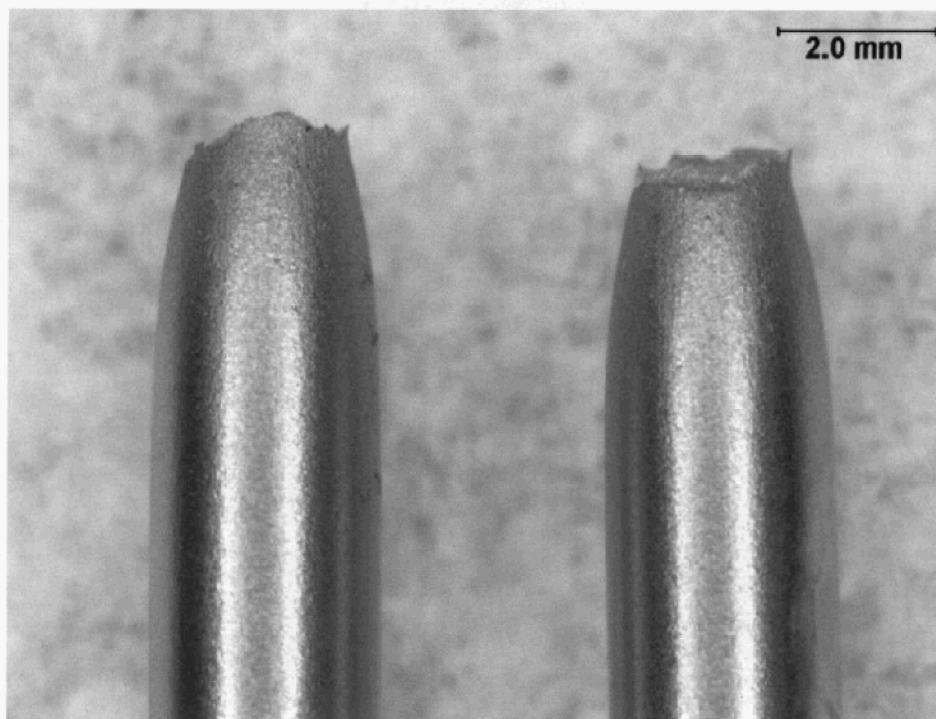


Figure 26: A stereo-micrograph of the sample from SSR 9: AY-102, pH 11, 77°C with applied potential of -750 mV vs SCE.

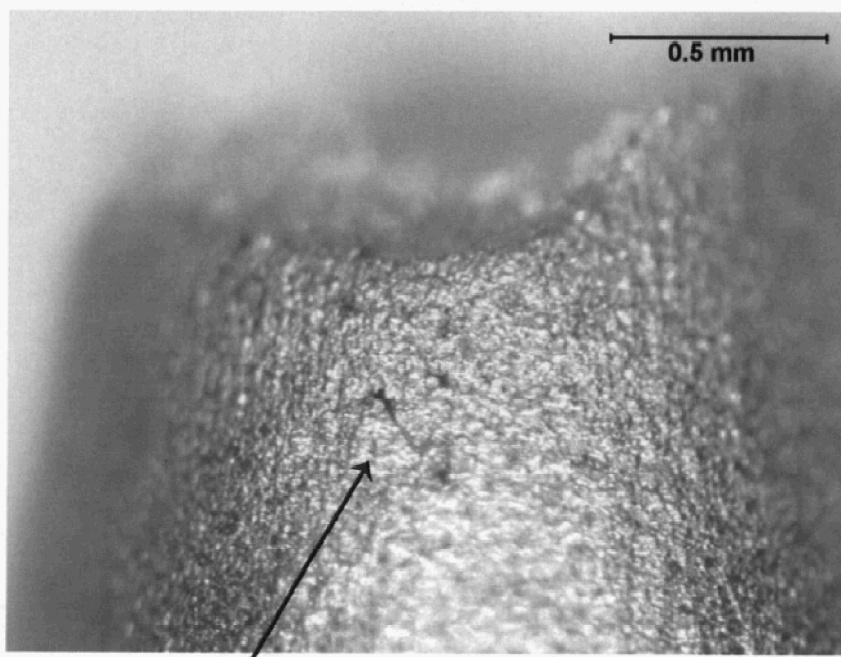


Figure 27: A stereo-micrograph of the sample from SSR 9: AY-102, pH 11, 77°C with applied potential of -750 mV vs SCE (close-up). Note the minute crack, as shown by the black arrow.

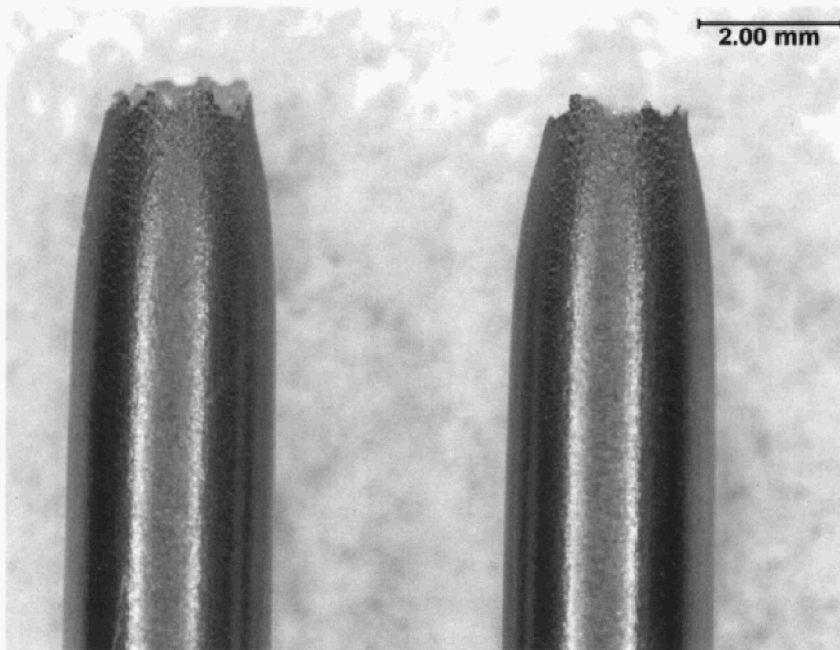


Figure 28 A stereo-micrograph of the sample from SSR 10: AY-102, pH 11, 77°C with applied potential of -775 mV vs SCE

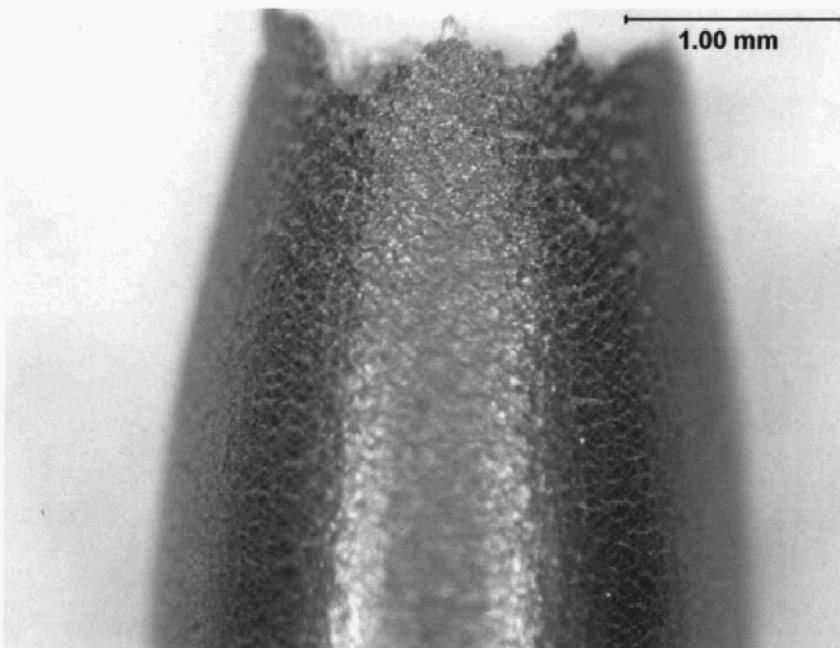


Figure 29 A stereo-micrograph of the sample from SSR 10: AY-102, pH 11, 77°C with applied potential of -775 mV vs SCE (close-up)

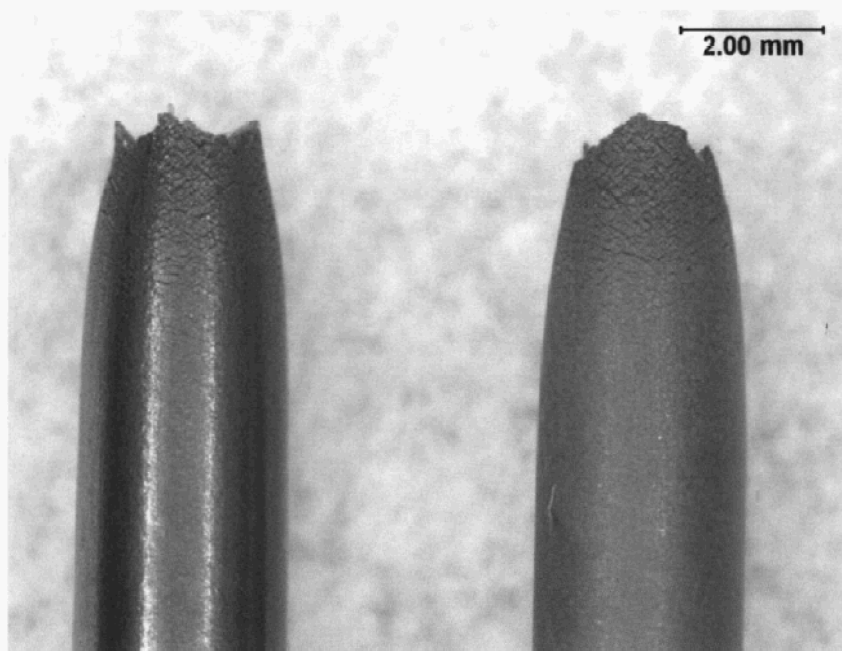


Figure 30 A stereo-micrograph of the sample from SSR 11: AY-102, pH 11, 77°C with applied potential of -800 mV vs SCE

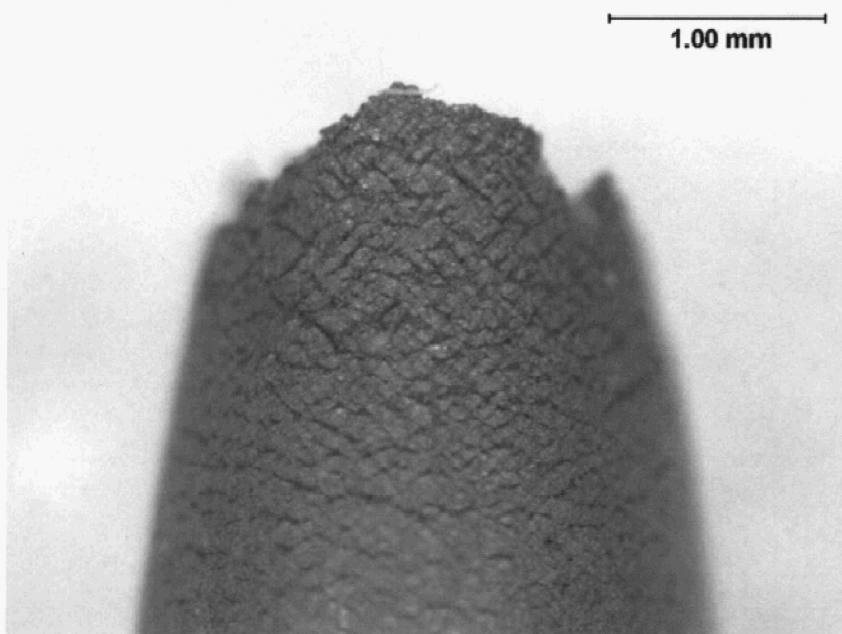


Figure 31 A stereo-micrograph of the sample from SSR 11: AY-102, pH 11, 77°C with applied potential of -800 mV vs SCE (close-up)

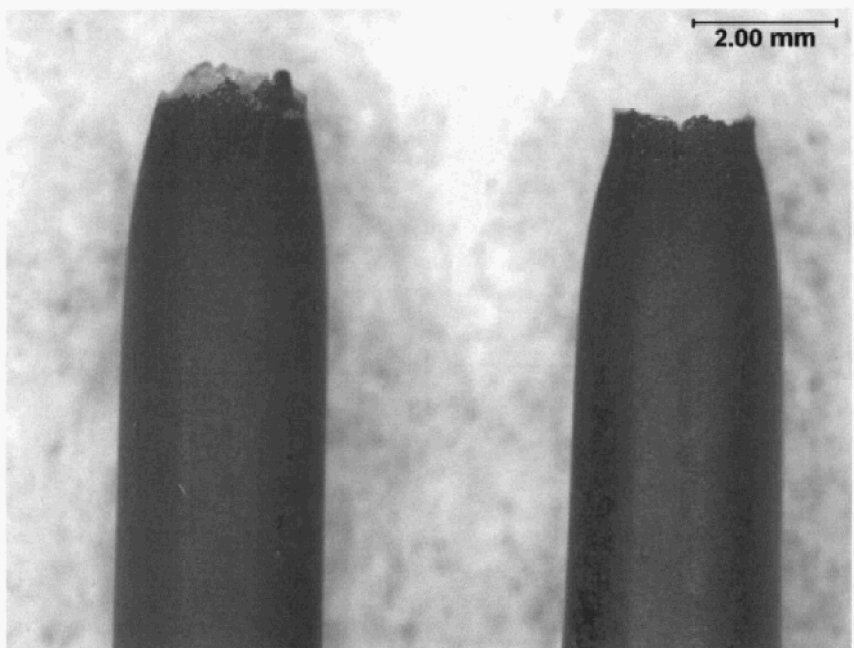


Figure 32 A stereo-micrograph of the sample from SSR 12: AY-102, pH 11, 50°C with applied potential of -775 mV vs SCE

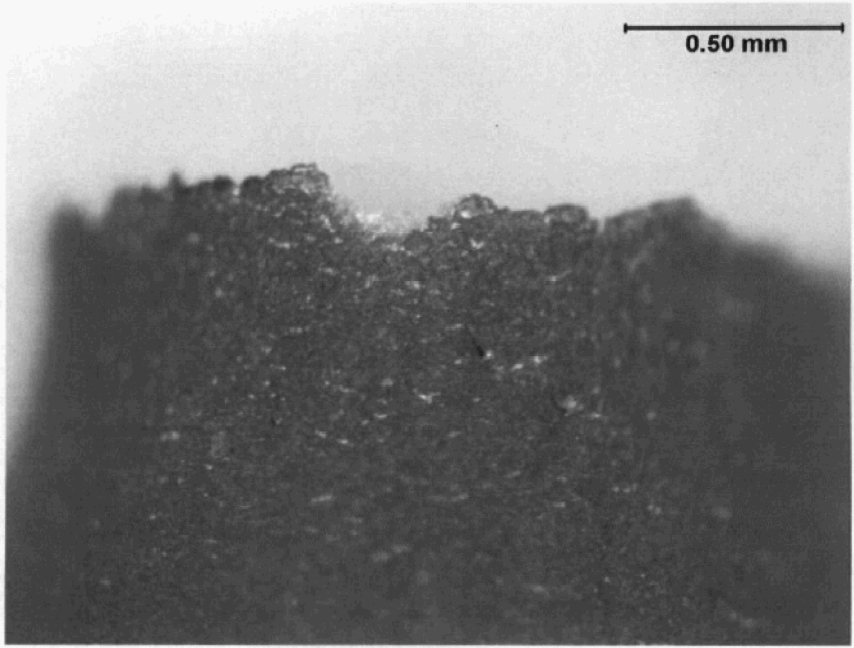


Figure 33 A stereo-micrograph of the sample from SSR 12: AY-102, pH 11, 50°C with applied potential of -775 mV vs SCE (close-up)

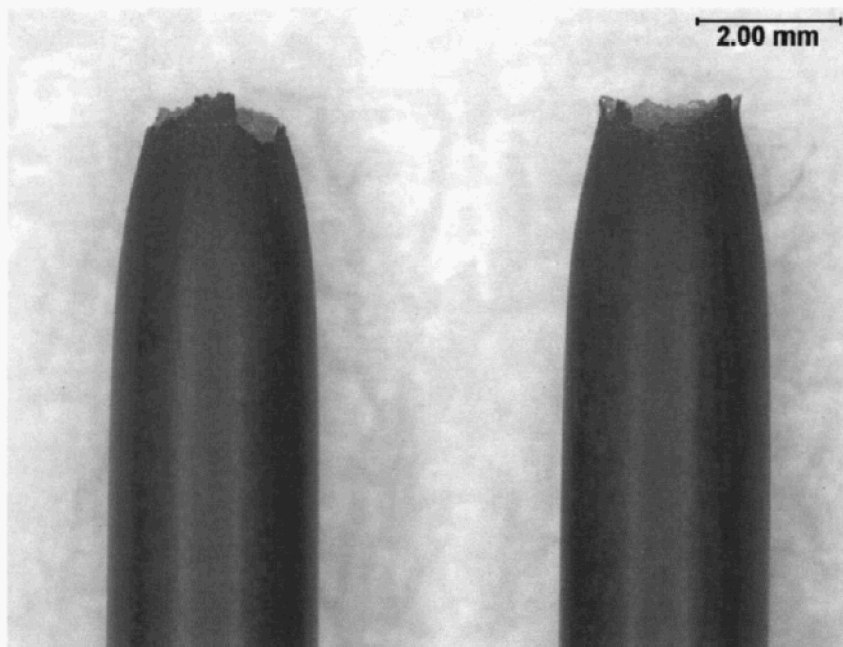


Figure 34 A stereo-micrograph of the sample from SSR 13: AY-102, pH 11, 50°C with applied potential of -800 mV vs SCE

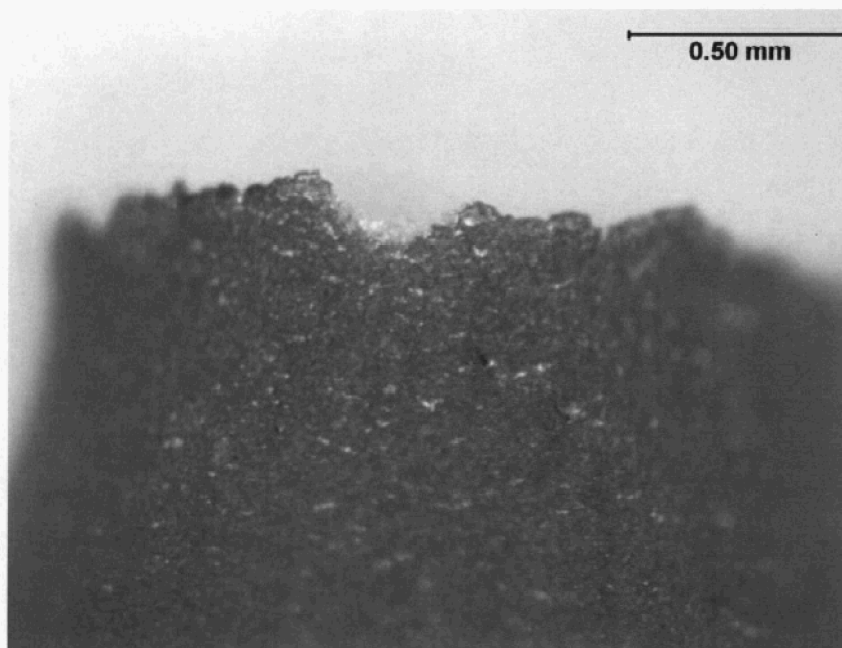


Figure 35 A stereo-micrograph of the sample from SSR 13: AY-102, pH 11, 50°C with applied potential of -800 mV vs SCE (close-up)